Author version
Energy Environ. Sci., 2019,12, 2054-2079
10.1039/C9EE00802K

Kinetic and material properties of interfaces governing slow response and long timescale phenomena in perovskite solar cells

Hongxia Wang,*[1] Antonio Guerrero,*[2] Agustin Bou,[2] Abdullah Al Mayouf,[3] Juan Bisquert*[2]

1 School of Chemistry, Physics and Mechanical Engineering, Queensland University of Technology, Brisbane, QLD 4001 Australia

2 Institute of Advanced Materials, Universitat Jaume I, 12006, Castello, Spain

3 Electrochemical Sciences Research Chair (ESRC), Department of Chemistry, Science College, King Saud University, Riyadh, Saudi Arabia

Email: hx.wang@qut.edu.au (H. Wang); aguerrer@uji.es (A. Guerrero), bisquert@uji.es (J. Bisquert)

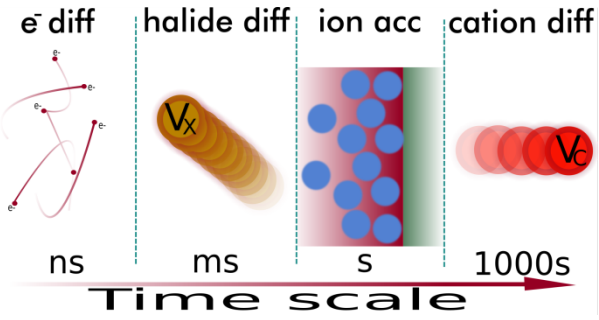

Abstract

The last decade has witnessed the skyrocketing progress of perovskite solar cells (PSCs) with its current world record energy conversion efficiency reaching over 24%. Nevertheless, unsatisfactory device stability and current-voltage hysteresis normally observed with most PSCs under operational condition are the bottlenecks that restrict the application of this photovoltaic technology in practice. It is known that interface properties are the heart of an electronic device performance. Understanding the interactions occurring at the interfaces is important to design and develop effective strategies to address these issues associated with PSC. In this review, we summarize the most recent advancement on understanding the interfaces in PSCs, in particular the interfaces of perovskite/electron transport layer (ETL) and perovskite/hole transport layer (HTL). Our main interest is to provide a guidance in the immense complexity of dynamic behaviours of the PSCs, particularly concerning the slowest time scale measurement that have a maximum impact in the actual operation of the solar cell. Therefore we address the separation of phenomena such as ion migration, interfacial charge accumulation, and surface electrochemical reactions. We provide an analysis of electrooptical small perturbation methods, including impedance spectroscopy (IS), and the description of negative capacitance, as well as spatially resolved techniques. The impact of different contacts with variable morphology, composition on the perovskite/ETL and perovskite/HTL interface properties reflected by kinetics of charge transport and chemical reactions are discussed to provide deep insights into the operational mechanism of PSCs. We reach the conclusion that a number of measurements observed in the time frame of 0.1 to 10 s are due to slow response of the ionic double layer, and we identify asymmetric surface charge and discharge processes responsible for such kinetic effects. We also suggest the research direction regarding new approaches to understanding interfacial reactions of PSCs to achieve high device performance in the future.

Broader context

While metal halide perovskite materials have shown outstanding properties for applications in photovoltaics and optoelectronics, the operation of the devices is hindered by a number of phenomena that occur on extremely low frequencies and long time, and have proved very difficult to characterize systematically. Based on an extensive overview of contact phenomena we show that the interface of the perovskite material with organic or inorganic contacts is a site where a combination of ionic and electronic phenomena conspire to produce effects that severely modify the expectations received from the traditional solar cell operation. Our analysis has three main aspects: the charge accumulation phenomena, the dynamic phenomena, and the physico-chemical features of the interface. From a review of a very broad range of methods and materials, we propose a general interpretation of the main factors dominating the response. In summary one can observe totally reversible phenomena of charge accumulation, a partial ionic binding that retards the response, and intense chemical interactions that perturb and invalidate the devices. Sorting out these phenomena is a key objective for ensuring stable performance and endurance in future technologies of metal halide perovskites.

1. Introduction

Semiconductor materials based on metal halide perovskite have received enormous attention owing to their exceptional opto-electronic properties which open for applications in areas such as solar cells, light emission diodes, X-ray detectors, etc. The chemical formula of the perovskite can be described as ABX_3 where A = monovalent cations such as methylammonium (MA), formamidinium (FA), cesium (Cs), B = divalent cations such as lead (Pb), tin (Sn) and X = halide anions including chloride (Cl), bromide (Br), iodide (I). $MAPbX_3$ was first synthesized by Weber in 1978.[1] The first attempt of applying methylammonium lead halide (bromide, iodide) ($MAPbBr_3$, $MAPbI_3$) in solar cells was reported by Kojima et al. in 2009, who employed the perovskite nanocrystals as light absorber in a conventional sensitized solar cell using iodide/triiodide based liquid electrolyte.[2] The past ten years have witnessed the skyrocketed progress of the power conversion efficiency of perovskite solar cells thanks to advancement in material engineering and interface optimization. The current certified record efficiency of PSC is 24 % for single junction solar cells, which is comparable to crystalline silicon solar cells and even surpass the efficiency of thin film CIGS and CdTe solar cells. Compared to the solar cells based on light absorber such as silicon, CIGS and CdTe, the most attractive feature for PSCs include low temperature solution processing methods and high efficiency achieved with very thin layer (< 500 nm), as well as the abundance of raw materials. These make it viable for large-scale production of light weight, flexible PSCs devices using cost-effective methods such as roll-to-roll, screen-printing or slot-die, achieving low cost solar electricity in the future.

It has been well established that in addition to the excellent bulk photovoltaic (PV) characteristics, the interface properties determine to a large extent the performance of a hybrid perovskite solar cell (PSC) device. A typical PSC device architecture is composed of fluorine-doped tin oxide (FTO)/electron transport layer (ETL)/perovskite/hole transport layer (HTL)/gold, which contains four interfaces. Different interface materials used in PSCs have been shown in recent reviews.[3-6] Moreover, it is often assumed that slow dynamic effects such as hysteresis in *j-V* curves is associated to ionic motion effect. However, a deterministic connection between the ionic displacement and the observed kinetic variations of the outer electronic current has not been established yet. In this review we will discuss the recent advances of understanding on dynamic properties of PSC devices in the time scales associated to actual operation of the solar cell. We argue that the actuation of ions on the contact interface is a predominant cause for different types of slow kinetic effects. We further connect these dynamic effects with chemical reactivity at the interfaces, which ultimately influence the device stability.

2. Timescales of ionic/electronic phenomena in PSC

The first question we ask is about the transport rates in a PSC. And not only electronic transport, as it has been well established that a significant amount of ionic

displacement influences the characteristics of measurement and operation of PSC.[7, 8] We are used to solar cells that are predominantly governed by electronic transport. For example, in silicon solar cells carrier transport is rather fast so that it is not likely to influence ordinary experimental observations, compared to recombination events.[9] This is why we can rely on energy diagrams that are solved with respect to a fixed background of ionic density.[10] On the other hand in solar cells made of nanostructured metal oxide the electron transport is considerably slower and transport resistance can be unambiguously determined.[11] In dye-sensitized solar cell diffusion of ions in electrolyte often forms a prominent feature, but it can be neatly separated from electron transport components by measurement protocols.[12, 13]

In the PSC, it has been found that many slow phenomena appear in physical measurements, the prominent representative being the hysteresis of current-voltage (*j*-*V*) curve.[14-17] A slow ionic transport is one possible reason for such sluggish response.[18] However, a clear connection between the rate of transport and the time response of PV properties has not been achieved, yet.

Recent work enables the quantification of ionic diffusion rates for lead halide perovskite materials, especially at room temperature. Methods such as the galvanostatic measurement,[19] impedance spectroscopy (IS), using the classical transmission line method,[20] and suppression of luminescence in laterally contacted electrodes,[21] have provided quantitative values of the diffusion coefficient of halide defects which is in the order $D_{V_I} = 1 \times 10^{-8}$ cm^2 s^{-1} for methylammonium lead trihalides perovskite (i.e. $MAPbI_3$ or $MAPbBr_3$). In addition, cation transport has also been measured for extrinsic Li^+ and MA^+. Alternatively, a variety of techniques operating in a wide array of frequency ranges have provided values of electronic mobility in metal halide perovskites.[22] While there is a scattering of values depending on many factors such as specific composition and preparation methods of the perovskite materials, it is safe to take some representative values that are indicated in Table 1.

Type	**Diffusion coefficient D (cm^2 s^{-1})**	**Carrier mobility μ (cm^2 V^{-1} s^{-1})**	**Measurements[a]**
Electron transport	0.3	$\sim 1 - 100$	Several methods like THzC, MWC, PLQ or SCLC[22]
Extrinsic Li^+	1×10^{-7}	4×10^{-6}	IS[23]
Halide vacancy transport (V_I^+)	1×10^{-8}	4×10^{-7}	Galvanostatic voltage measurement,[19] IS,[20] PL suppresion.[21]

Table 1. Some characteristic kinetic coefficients in PSCs based on $MAPbI_3$ or $MAPbBr_3$, at room temperature. *a* lists the technique used to determine the mobility value: i.e. THzC: optical-pump-THz-probe photoconductivity, MWC: Microwave conductivity, PLQ: PL quenching method, SCLC: Space-charge Limited Current, IS:

Impedance spectroscopy.

The carrier conductivity (associated to the transport resistance) is the crucial quantity controlling possible power losses and determining which species govern carrier redistribution in application to external perturbation. A figure of merit that shows which current (either ionic or electronic) will be dominant in each situation is the quotient of conductivities. Considering electronic density *n* and ionic density *c* we expect that

$$\frac{\sigma_e}{\sigma_i} = \frac{\mathrm{n}\mu_e}{c\mu_i} = 10^7 \frac{n}{c} \quad (1)$$

This result indicates that in any typical situation the current is mostly driven by electronic current, unless the density of mobile ions becomes many orders of magnitude larger than electronic density. The latter may be expected in the dark in extremely low doped samples.

Starting from the previous general considerations, we may now compute several time constants that describe characteristic phenomena in the hybrid perovskite materials. In order to establish the relative significance of transport phenomena in the kinetic timescale, it is necessary to choose a characteristic distance. A good point to start our analysis is to consider the kinetic of transport of ionic carriers across a region with thickness of d =100 nm. The transit time for each carrier to diffuse across such a distance is

$$\tau_{diff} = \frac{d^2}{D} \quad (2)$$

The results for a typical solar cell layer with thickness in the order of hundreds of nanometers are shown in Table 2 and summarized in Figure 1. For ionic transport, this will be the time needed for ionic carriers consisting on halide vacancies to cancel a new composition gradient that occurs under external variations, and it takes the value $\tau = 10^{-2}$ s.

It is quite frequently found in PSC a much lower time scale for changes of variables like photovoltage or photocurrent.[16] Here this kinetic phenomenon with $\tau = 10^0 - 10^2$ s is attributed to ionic double layer kinetics, as it will be discussed later on. Finally, another type of migration occurs in the time scale of many hours ($\tau > 10^3$ s) which can be associated to much less mobile cation species MA^+.

Type	**Time**
Electronic transport across d =100 nm	$\tau = \frac{d^2}{D} = 10^{-9}$ s
Halide vacancy diffusion over a distance d =100 nm	$\tau = \frac{d^2}{D} = 10^{-2}$ s
The response of ions accumulated at the perovskite surface	$\tau = 10^0 - 10^2$ s

Cation vacancy diffusion over a distance d =100 nm	$\tau = 10^3$s

Table 2. Some characteristic timescales of kinetic phenomena in PSCs $MAPbI_3$ and $MAPbBr_3$, at room temperature.

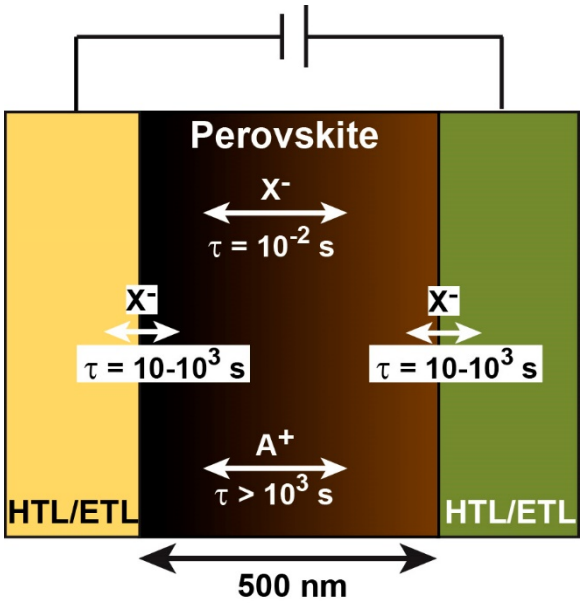

Figure 1. Representative characteristic times for ionic phenomena in a typical perovskite solar cell.

3. Fast Ionic transport in the bulk of the PSC

Ionic transport has emerged as a key player in perovskite research but its precise role in the slow response observed during electrical measurements and its relationship with degradation dynamics is under debate. On the one hand, there are strong evidences pointing to a fast ionic transport in lead halide perovskites. An alternative measurement to the solar cell diode is a planar configuration with lateral contacts that provides transport distance of hundreds of μm. In such system the analysis of the PL by excitation at 35 mW/cm^2 under applied bias reveals the formation of a dark front that advances with time (Figure 2).[21] Note that the applied voltage is similar to those at the maximum power point in working PSC. In addition, it is observed that the material becomes resistive as the dark front advances, indicating that doping is reduced in the dark area. Therefore, it is clear that techniques with spatial resolution are required to unambiguously correlate electrical measurements with electronic/ionic response.

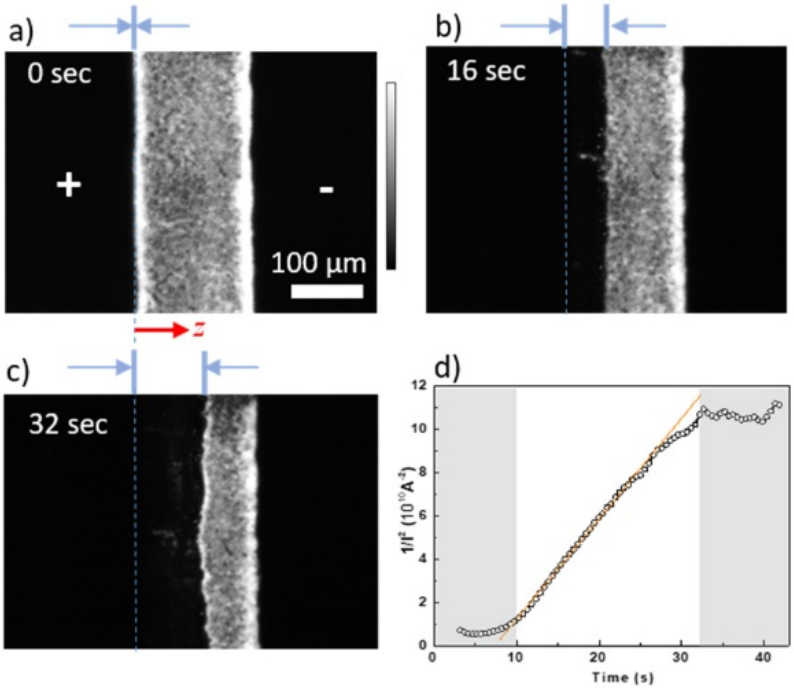

Figure 2. (a-c) Time dependent PL images of a perovskite film $CH_3NH_3PbI_{3-x}Cl_x$ measured under an external electric field of ~2×10^4 V/m interdigitated configuration with a channel width of ~150 µm. (d) $1/I^2$ monitored as a function of the time during the measurement of experiment a). Adapted with permission from reference [21].

On the other hand, a careful analysis of the timescale of the ionic movement in the bulk of the perovskite layer highlights that ionic transport towards the interface cannot be the main reason that is responsible for the slow electrical response observed in PSCs (i.e. hysteresis). In particular, simultaneous analysis of the measured current during the previous PL experiment allows the calculation of the diffusion coefficient of the migrating iodine vacancies.[21] A value of $D = 1 \times 10^{-7}$ cm^2 s^{-1} leads to ionic transit times through a perovskite layer of 100 nm in the order of miliseconds. This ionic migration timescale has also been confirmed by another spatially resolved technique like transient Kelvin probe force microscopy (Tr-KPFM).[24] Alternatively, *j-V* measurements are carried out at scan rates that typically take several seconds. Therefore, it is clear that activated ionic transport in the bulk of the perovskite layer is only one requirement to observe hysteresis but not the main reason. Indeed, all evidences point to the chemical and physical interactions of these migrating ions with the external interfaces as the main reason for hysteresis observation. For example, a thin layer of PCBM placed on the top of TiO_2 is able to completely suppress the measured hysteresis in the *j-V* response of devices with activated ion migration in the bulk of the material like $MAPbI_3$.[25] In the next section, we will describe the evidence for ionic accumulation at the surface of the PSC, and later we discuss the methods of observation of the kinetics of the surface charge.

4. Ionic effects at the interface

Under applied bias ions rapidly reach the external interfaces, with formation of an electrical double layer as it is well known in solid state electrochemistry. The combination of ionic an electronic phenomena such as space charge, interfacial electron transfer and ionic reactivity, leads to several possible types of physical and chemical interactions at the interfaces. There are different time resolved electrical techniques that can be used to decouple ionic and electronic response such as Impedance Spectroscopy which has been widely used in PSC. For example, pure ionic contribution with the classical transmission line for ion migration is observed during the measurements of $MAPbBr_3$ monocrystals (Fig. 3a). This technique measures the electrical response in the frequency domain separating resistive and capacitive contributions (or charge accumulation). A useful method to represent the impedance data is the complex impedance plot where x-axis (*Z*') is related to resistive elements and the y-axis (-*Z*'') to capacitive elements. A resistive element connected in parallel to a capacitor (RC) leads to an arc in the complex impedance plot. The most common feature in the impedance spectra of a PSC is the appearance of two arcs as shown in Figure 3b. The data can be fitted to the equivalent circuit shown. Both resistances R_1 and R_2 correspond to losses from both bulk and interfacial recombination.[19] Moreover, both have the same trends as a function of photovoltage or light intensity, indicating that they have a common origin. In contrast, the source of capacitances is clearly different. The Capacitance-Frequency (*C-f*) plot of the IS data is very useful to understand the capacitive contributions and correlate the charge accumulation with the characteristic time of the physical process. It has been established that there are two plateaus indicating well-differentiated capacitances the *C-f* plot of PSC, Fig. 3b. The high frequency capacitance C_g is the dielectric capacitance,[26] related to the bulk polarization, and the low frequency capacitance C_s corresponds to surface accumulation processes.[21] The fact that C_s changes when different configurations are used is a strong evidence for the existence of a surface capacitance. A similar behaviour is observed in perovskite quantum dot films.[27]

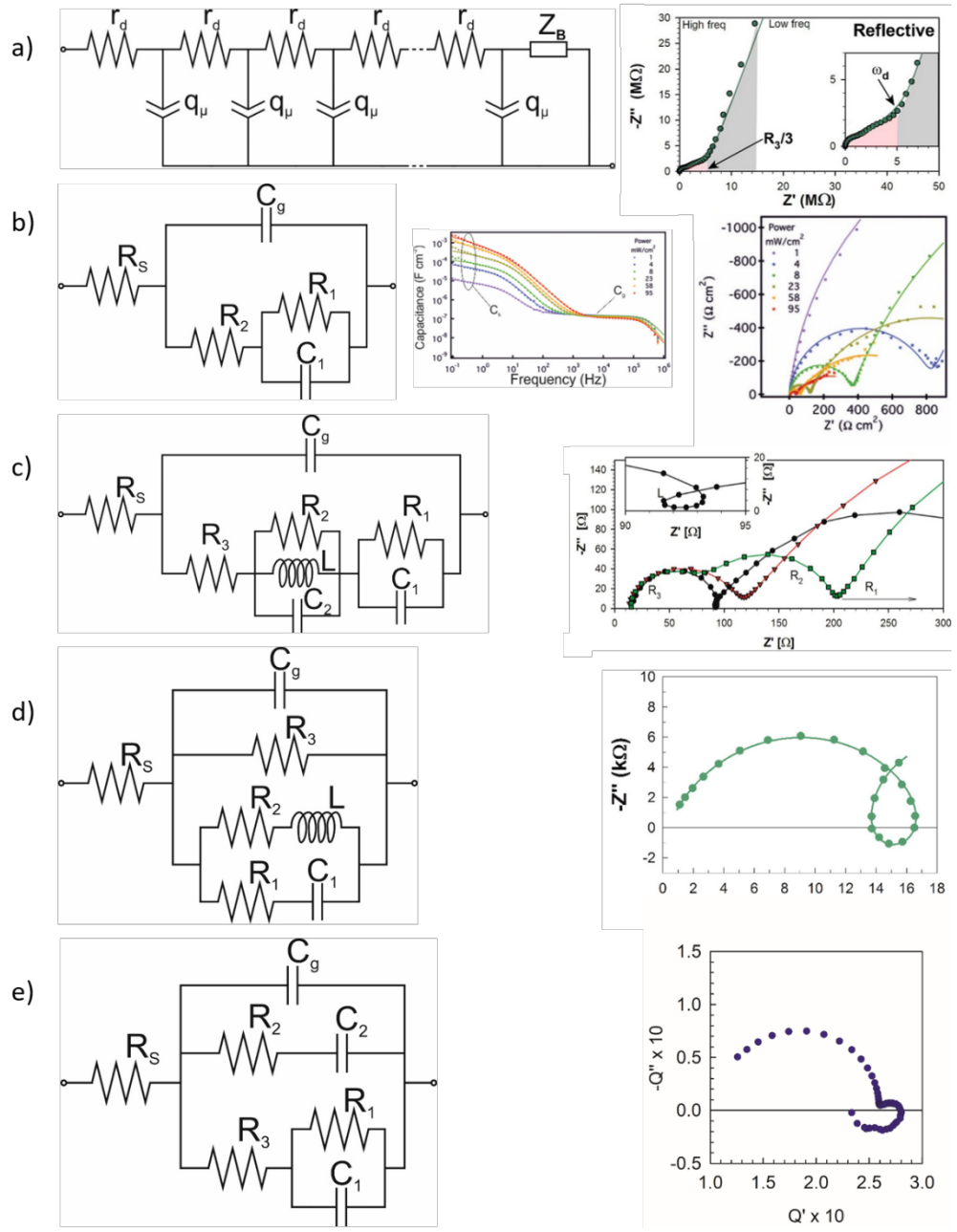

Figure 3. Summary of equivalent circuits used for the analysis of impedance spectra of perovskite solar cells with examples of representative spectra for each circuit. Here, we use the following notation for capacitances: C_g is the geometrical capacitance, C_1 is the low frequency capacitance usually associated with accumulation, C_2 is the intermediate frequency capacitance; and for resistances: R_S is the series resistance, R_1, R_2 and R_3 are always ordered from the lowest frequency resistance to the highest, starting from 1. (a) Transmission line showing impedance of ion diffusion in a finite layer used for ionic transport quantification in perovskites, highlighted in red. Reproduced with permission from [20]. (b) Equivalent circuit used for two arcs spectra. Here we show capacitance spectra depending on light intensity. Reproduced with permission from [28]. (c) Equivalent circuit used for three arcs spectra and intermediate frequency loops; here,

resistances appear in series. Reproduced with permission from [31]. (d) Equivalent circuit used for spectra with two arcs that vary in concordance which have exotic features such as inductive loops or negative capacitances; here, resistances appear in parallel. Reproduced with permission from [64]. (e) Equivalent circuit obtained from the analysis of both IS and IMPS data together; here we have resistances in parallel as well as in series. Reproduced with permission from [79].

The features of low frequency capacitance in metal halide PSC have been broadly studied and a general characteristic picture has emerged. The fact that ions migrate across the bulk under voltage bias or light soaking is well known. When ions arrive at the interfaces, they accumulate there. A main component of the double layer is the Helmholtz layer, formed by the ions in contact with the electrode surface, which provides a capacitance of the order of 10 μF cm^{-2}. However, there also is a diffuse double layer, that contains a surface charge[29]

$$Q_{diff} = \frac{2\varepsilon\varepsilon_0 k_B T}{qL_D} \sinh\left(\frac{q\Delta\varphi}{2k_B T}\right) \quad (3)$$

This charge is distributed in the typical distance of a Debye length for the electrode surface,

$$L_D = \left(\frac{\varepsilon\varepsilon_0 k_B T}{q^2 N}\right)^{1/2} \quad (4)$$

In Eqs. (3) and (4) the standard symbols have their usual meaning.[30] Δφ is the potential drop across the double layer, and *N* is the net underlying ion density in the bulk.

Zarazua et al.[28, 31, 32] showed by analysis of the evolution of C_s with V_{oc} that the surface capacitance C_s is actually an accumulation capacitance, however, it depends on the accumulation of both ionic and electronic carriers and is highly dependent of the specific binding of the perovskite to the contact surface. In this line, direct evidence for the intimate connection between surface capacitance and hysteresis emerged by comparing normal and inverted version of PSC as indicated in Fig. 4a.[33] The cells with PCBM electron contact display a much lower low frequency capacitance than those with TiO_2 contact. And correspondingly, *j-V* cycling hysteresis is significantly reduced in the inverted cell. Further evidence for this strong correlation has been obtained by measuring dark currents at different scan rates as shown in Fig. 4b and 4c.[34] By modification of the device configuration it is possible to suppress the capacitive contribution of the current. The square-like response is removed in a configuration that avoids the use of metal oxides based ETL (Figure 4c). This is further confirmation that the surface capacitance is a composition of ionic and electronic carriers accumulated at the interface and highly depends on contact interfaces of perovskite/charge extraction layer.

The raise of capacitance at low frequency has been interpreted in many cases as the manifestation of bulk traps. However a recent study[35] using the analysis of low

frequency noise has found that the capacitance does not scale with thickness, in agreement with the previous scaling properties obtained by impedance spectroscopy.[36]

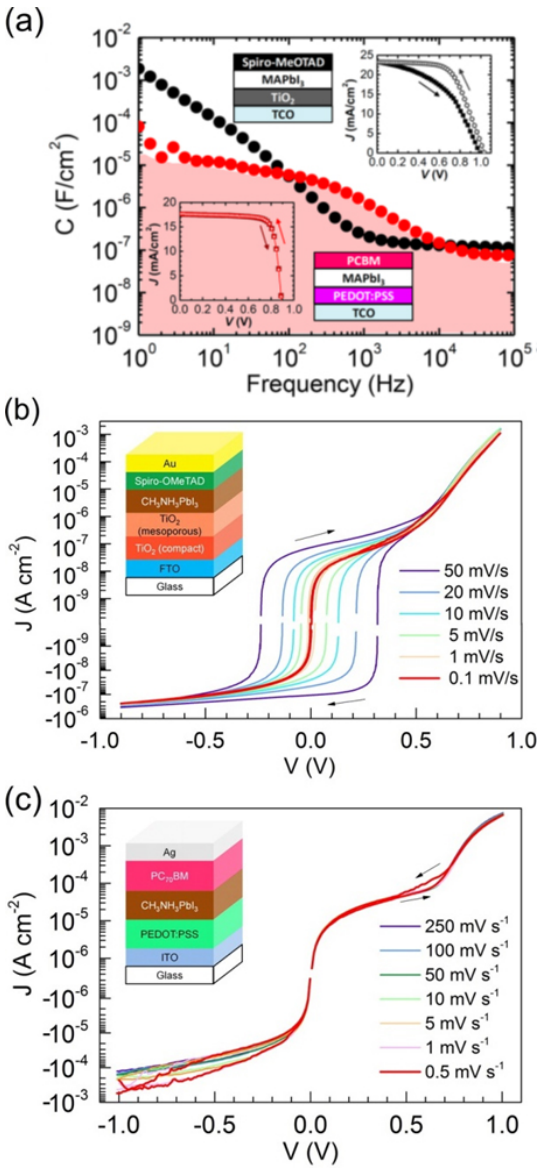

Figure 4. a) Capacitance-Frequency plot under one sun illumination at short-circuit condition (bias voltage = 0 V). The normal and the inverted structures represent cp-TiO_2/$MAPbI_3$/spiro-MeOTAD and PEDOT:PSS/$MAPbI_3$/PCBM, respectively. Reproduced with permission from [33]. b) and c) Dark J–V curves measured at different scan rates with corresponding structures sketched in the insets. The positive currents are forward bias direction. Reproduced with permission from [34].

Metal oxides based ETLs typically lead to large surface capacitances and hysteresis as shown above. The impact of TiO_2 compact layer thickness on the hysteresis behavior of carbon based HTM-free PSCs was confirmed by Han et al.[37] By tuning the thickness

of spray-deposited TiO_2 layer over a few nanometers, the hysteresis behavior of the perovskite was switched from inverted to hysteresis-free and then to normal (Figure 5). The combined effect of dynamic of charge accumulation and charge recombination are believed to be responsible for the observed behavior.

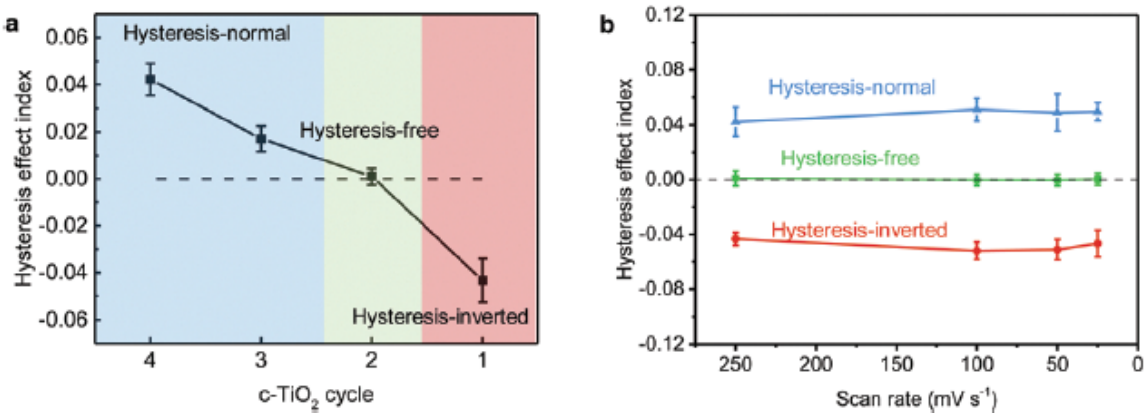

Figure 5. Dependence of hysteresis effect index on (a) c-TiO_2 layer spray deposition cycles and (b) scanning rates for hysteresis-normal, hysteresis-free and hysteresis-inverted devices. Reproduced with permission from [37].

The dependence of capacitance on frequency in organo-metal halide perovskite shows a range of features as discussed before, but it has been concluded that low frequency domain is mainly associated with surface capacitance. It is therefore expected that slow kinetic changes of the surface will provide measurable evolution of the capacitance value. Garcia-Belmonte and coworkers have been able to identify the surface depletion layer capacitance and the subsequent Mott-Schottky plot.[38] However, they have found that the surface depletion layer capacitance is affected by a large extent of hysteresis when the applied voltage undergoes a scan cycle (Figure 6). These results are important as they reveal the electrical response at the proximity of the contact, and this is a manifestation of surface attached species, i.e., a change of surface charge that occurs on a much longer scale than the measurement of the capacitances.[39]

In summary, once the ions complete the accumulation, their responses to the small perturbation are slow, with characteristic times related to the low frequency capacitance. In a later section we argue that this surface polarization takes longer to be discharged than the time it takes for charging, in phenomena connected to surface attachment and electrochemical surface reaction.

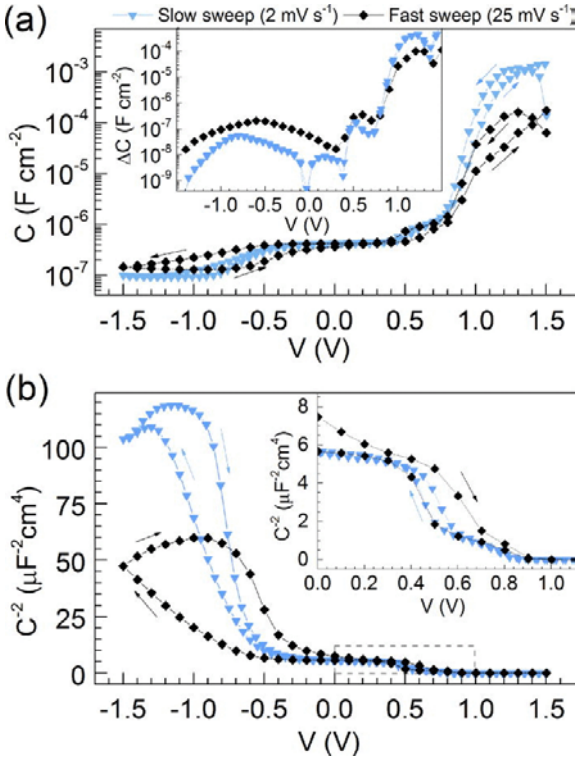

Figure 6. (a) Capacitance-voltage curve and (b) respective Mott-Schottky plot of a $CH_3NH_3PbI_3$-based PSC with mesoporous TiO_2 matrix for a larger DC bias window at different scan rates, as indicated. Inset in (a): the corresponding capacitance absolute difference between scan directions ΔC. The inset in (b) is the typical Mott-Schottky plot region, pointed inside the dashed gray square. Reproduced with permission from [39].

Due to the complexity of the surface phenomena it is important to adopt complementary measurement techniques that may validate specific assumptions. Photoluminescence (PL) measurements of more simple configurations containing only one perovskite/contact interface can also unveil information on the properties of the perovskite/external contact interfaces. In early work, it was found a large drift of PL intensity that persists over 20 s.[16] Measurements by Lundt *et al.*[40] revealed dramatic modifications of PL depending on the treatment of the exposed perovskite surface (Fig. 7). Significant PL quenching occurs with the deposition of 1 nm C_{60} that could be interpreted by passivation of surface traps. However, a similar effect occurs when using an amorphous thin organic buffer layer between the perovskite and the C_{60} but not when the thin layer is used without C_{60}. Therefore, the PL quenching is attributed to the formation of space charge, which is associated to electron capture in C_{60} and compensating ions in the perovskite side.

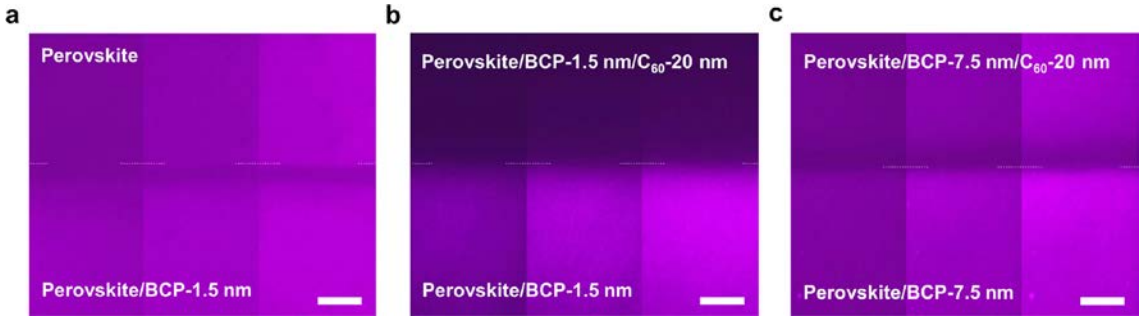

Figure 7. Time-resolved fluorescence microscopy images of perovskite film with (a) bare perovskite, (b) 1.5 nm amorphous buffer layer spacer with 20 nm C_{60}, and (c) 7.5 nm buffer layer spacer with 20 nm C_{60}. The buffer layer-only coated perovskite film is provided in each panel for reference. The time scale is 0 s (left), 30 s (middle), and 60 s (right) for each figure; the brightening of the PL with time stems from space-charge accumulation that increases radiation recombination rates. The dashed line is used as guide to the eye to indicate the interface position. The scale bar is 100 μm for all figures. Reproduced with permission from [40].

Recently, the critical effect of ions present at the ETL/perovskite interface has been highlighted for the wide band gap perovskite based on $MAPbBr_3$.[41] The ETL was treated with additives containing Li^+ to reduce undesired interfacial recombination processes at the $MAPbBr_3/TiO_2$ interface. An emission peak at 670 nm (Fig. 8) was identified with interfacial recombination from the TiO_2 to the perovskite layer which could be suppressed by doping the TiO_2 with a salt containing Li^+. It was proposed that the presence of Li^+ atoms at the ETL increases the cation density at the hole accumulation zone, thus increasing the size of the space charge layer. Therefore, the surface density of electronic holes at the critical zone of the surface of the TiO_2 layer is reduced, as indicated by the decrease of charge-transfer radiative recombination observed at 671 nm and the simultaneous increase in the band-to-band emission of perovskite. Reduced recombination was confirmed by IS and electroluminescent measurements.

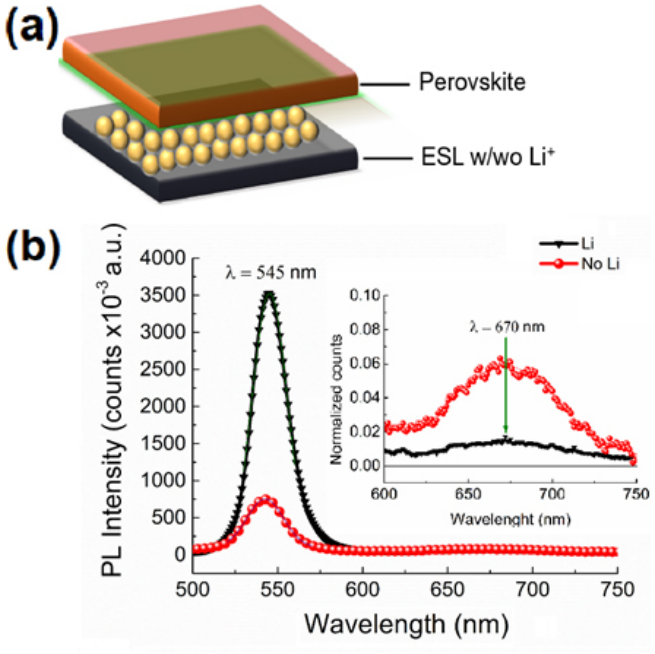

Figure 8. Photoluminescence measurements focused in both TiO_2/perovskite showing the enhancing of perovskite emission and suppression of the interfacial emission. PL spectra obtained under continuous wave (CW) excitation (λ_{exc}=380 nm, I_{exc} = 10 mW cm^{-2}) of devices with (black) and without (red) lithium treatment at metal oxide contact. Inset plot shows the quenching of the second feature when lithium is present at metal oxide contact. Reproduced with permission from ref. [41].

5. Electronic effects at the interface

Although the ionic effects have grabbed the attention in the perovskite community because of their peculiarity, electronic phenomena remain one of the keys for improving device performance. While bulk electronic phenomena such as carrier diffusion or bulk recombination are well established advantages of perovskite materials,[42] interfacial phenomena such as traps, surface recombination and charge extraction remain a big issue to completely achieve high and stable performances.[43] Thus, choosing adequate materials as extraction layers is a crucial issue.

When selecting a material for extracting carriers, energy level alignment provides a dominant criterion to produce a good selective contact.[44, 45] In the case of perovskites, this is not an easy question, since the energy level of the perovskite itself is strongly dependent on the composition (i.e. different halides or cations), surface termination,[46] the surface state charging,[47] and even on the preparation method.[48] Actually, perovskite energy levels may change depending on the substrate on which they are prepared, as shown by Miller et al. using photoemission spectroscopy.[49] In fact, substrates may change doping densities and may turn the perovskites from n-type to p-type. Both for ETL and HTL, there are some materials that have been widely used because of their suitable properties, Figure 9.

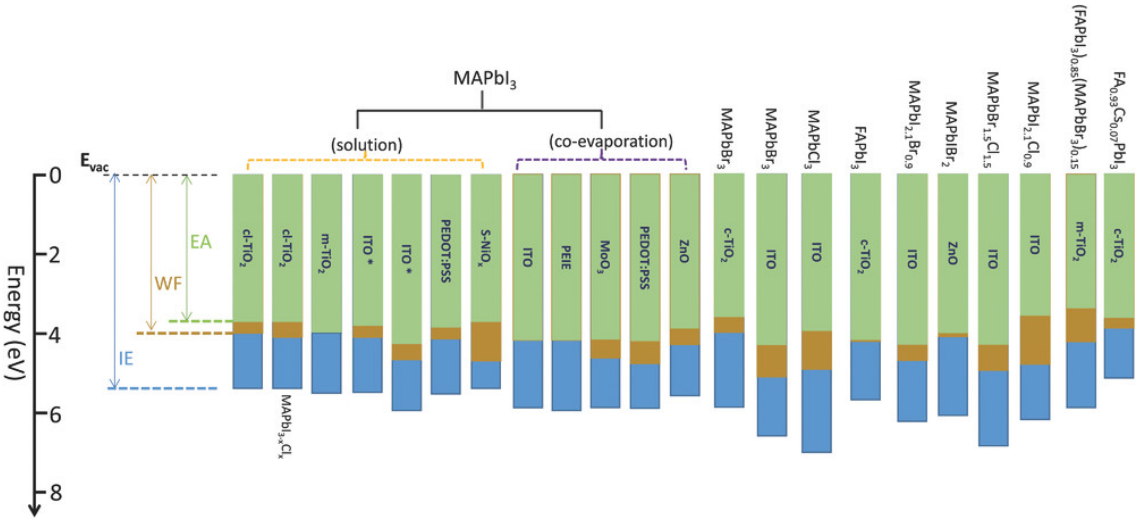

Figure 9. WF, IE, and EA values for various perovskites reported by different groups, which are prepared either on different underneath layers and/or by different methods. The listed materials on the bars are the substrates, and the types of perovskite materials are listed on top. WF and IE are derived from UPS measurement, while EA values are derived from transport gap or optical bandgap. The star symbols (*) represent that the work used the same preparation method and the same substrate material but reported in different literature. Reproduced with permission from [48].

On the one hand, for the ETL there are two main options, metal oxides (such as TiO_2, SnO_2 or ZnO) and organic layers (such as C_{60} or PCBM). In the case of metal oxides, it is the TiO_2 the one that has been more widely used, giving high efficiencies both in planar and mesoporous layers. However, the TiO_2-perovskite interface has given substantial problems like charge accumulation[32] and hysteresis.[14] Despite a good energy level alignment, charge extraction problems, surface non-radiative recombination and charge accumulation, have been found to limit the device performance. Partial solutions to those problems have been found via TiO_2 doping with different materials. Liu et al. reported free hysteresis PSCs by doping TiO_2 with lithium, reducing the density of electron traps and increasing conductivity.[50] Tan et al. proposed contact passivation by using chlorine capped TiO_2 colloidal nanocrystal film, reducing interfacial recombination.[51] In general, contact modification of TiO_2 is needed to suppress undesired interfacial processes via doping or passivation.[52-54] ETL-perovskite band alignment is really sensitive to all the electronic processes that occur in the interface, and may change the interface capacitance in some orders of magnitude.[55] Extended information about the chemical modifications of the contact is provided in section 9.

The hypothesis of surface electronic traps causing hysteresis[43] is difficult to distinguish from an ionic binding or surface polarization and relaxation effects, since surface capacitances would be high as well in the case of surface electron traps. However, some changes of ionic species affect strongly the capacitance onset over the Helmholtz layer, and it seems unlikely to invoke a passivation of traps to explain such

effect.[41] The predominance of an electrostatic effect caused by ion distribution has been explicitly shown using ultrathin buffer layers in PL experiments, as commented in Figure 7.

On the other hand, two main materials are used for the HTL side generally: Spiro-OMeTAD and PEDOT:PSS, although there is ongoing research into finding suitable materials, which are usually organic. As commented before, perovskite energy levels change with perovskite composition. These changes are significant in the perovskite valence band, but the conduction band changes are smaller. It is then important to change HTL characteristics to get good band alignment.[56] One of the reasons why spiro-OMeTAD is widely used is the fact that it allows energy level changes by oxidation, thus being a versatile option.[57] Gelmetti et al. recently analyzed the behaviour of different organic HTLs with chemical structures similar to those of the spiro-OMETAD but different energy levels, and demonstrated that the HOMO energy values differ importantly when depositing on top of the perovskite layer having an impact in the V_{oc}, which justifies the difficulties in finding an appropriate HTL material.[58] Nevertheless, problems with perovskite-HTL interface also relates to reactivity and degradation in addition to energy level alignment, and this is discussed further in a later section.

A classical question about PV operation mechanisms is whether the work function difference between the electron and hole contact materials correlates with the open circuit voltage. Energy alignment at the contact is important to produce a good selective contact, but once this is achieved, the local adaptation in the contact region makes V_{oc} quite independent of the overall built-in voltage. A striking demonstration[59] is presented in Figure 10, where cells with widely different work function at the ESL show very similar PV characteristics, mainly differing in FF.

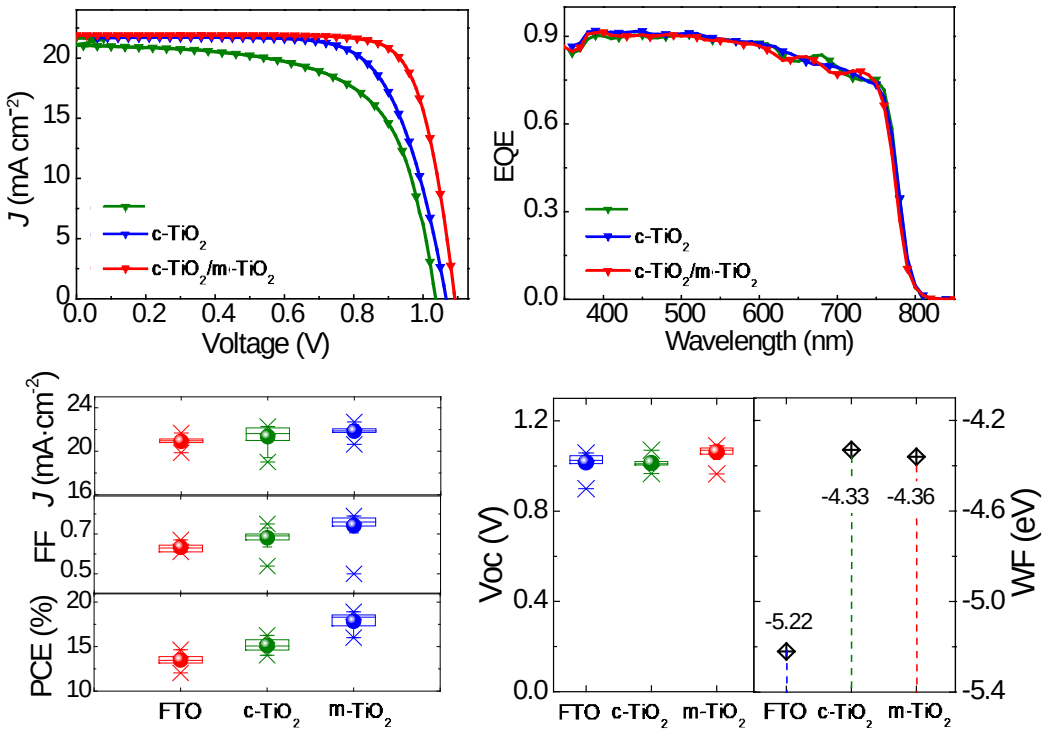

Figure 10. (A) Current-voltage (j−*V*) curves measured under 1 sun illumination and (B) external quantum efficiency (*EQE)* of representative perovskite solar cells containing meso-TiO_2, c-TiO_2 and *ETL-free* architectures. (C) Summary of device parameters obtained for more than 40 cells measured under AM1.5G sun illumination, room temperature and air conditions. (D) The open circuit voltage in comparison to the work function of the different contact layers. Reproduced by permission from [59].

6. Dynamic effects and time constants

In the section 4 we have outlined several phenomena that point to the strong experimental manifestation of accumulation of ionic and electronic charge in the contacts of the device. The interface of the perovskite with the contact appears a critical site controlling these phenomena. In order to classify and understand these interfacial phenomena it is important to attribute an interpretation to kinetic constants that describe the changes of the surface conditions, in the context of a variety of phenomena indicated in Table 2.

A brief light soaking treatment produces drastic changes in the Open circuit voltage decay (OCVD) as shown in Figure 11.[60] In these experiments the V_{oc} of the device is monitored after light is turned off for different pre-treatment light soaking time (Δt). The effect of light seems to be similar to that observed under a voltage bias stimulus. The OCVD is slow for a device that has not been light soaked previously and as expected for a solar cell the devices is able to obtain a null V_{oc} in the dark. Alternatively, a device that has been light soaked shows a fast V_{oc} decay but a persistent potential remains in the device indicating that migrating ions interact with the external contacts to create an

electrostatic potential. The construction of an additional voltage that persists on a long time scale is attributed to the partial attachment of cations to the surface during the short treatment of pre-illumination.

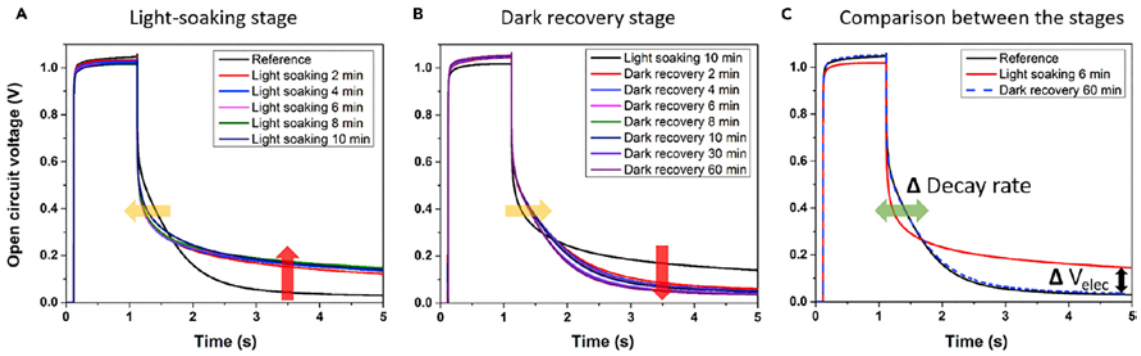

Figure 11. Top row: Open circuit voltage decay (OCVD) data for a PSC with a $TiO_2/CH_3NH_3PbI_{3-x}$ Cl_x Interface. (A and B) Changes in the decay rate appear in the light-soaking stage (A) and slowly revert back during the dark recovery stage (B). (C) An exemplary comparison of three OCVD measurements that show the two photo-induced changes in the decay rate and the buildup of an electrostatic potential, V_{elec} . Reproduced with permission from [60].

The energy diagram at the TiO_2/perovskite contact at four different stages of illumination condition shown in Figure 12 indicates a microscopic interpretation of the changes undergoing at the interface and the associated observation of cell voltage. For fresh devices measured in the dark, and for light soaking experiments using short times (Δt = 1 s) band bending is related to a depletion layer at the perovskite region close to the TiO_2, leading to flat bands at open circuit conditions under illumination. Under light soaking conditions, migration of positive cations and iodine vacancies is induced, generating the accumulation regime at the interface. The combination of ionic charge and hole concentration at the perovskite side of the interface forms an electrostatic potential as a result of the electric field across the interface. This potential is added to the built-in potential, and persists for a considerable time when illumination is suppressed due to ions remaining in the double layer region. The structure of surface polarization considering a combination of electronic and ionic mobile species can be established by a proper numerical analysis.[61] The role of ions in the formation of accumulation layers needs to be quantified to know the structure of the energy diagrams across the PSC. A study with different Hole Transport Layers (HTL) shows that a good alignment not only suppresses the hysteresis, avoiding charge accumulation at the interfaces, but also degradation of the hole transport layer is reduced.[62]

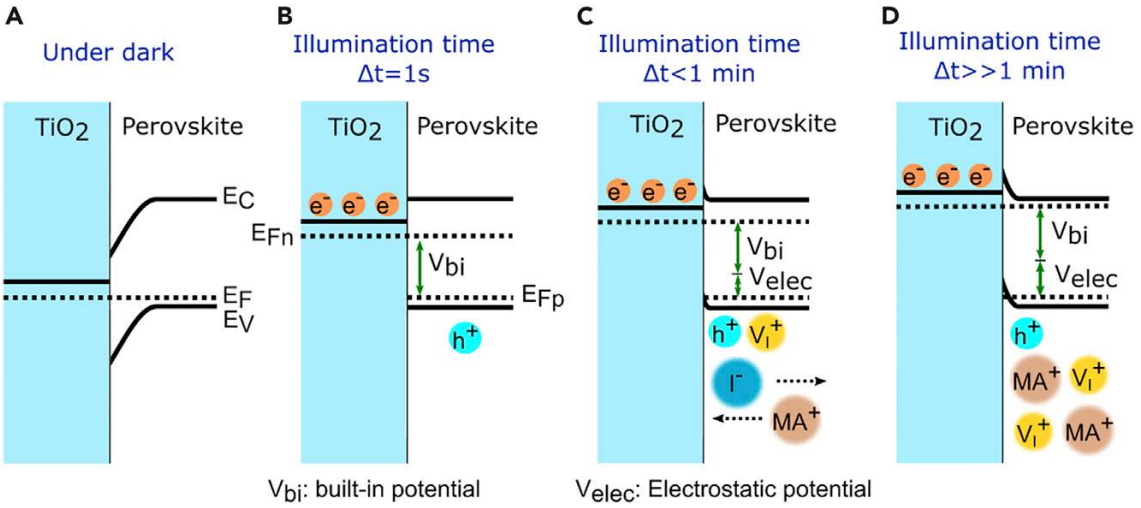

Figure 12. The energy diagram at the TiO_2/perovskite contact at four different stages. (A) In the dark, (B) At a very short illumination time of $\Delta t = 1$ s. (C) At an illumination time close to 1 min. (D) After a substantial illumination time of $\Delta t > 1$ min. This potential is added to the built-in potential. Reproduced with permission from [60].

An electrical model that relates the surface polarization and the electrical response during the *j-V* measurements has been developed.[63] The scan from forward to reverse voltage produces a bump in the current due to the slow release of the surface attached charge. This is described by an equation of the type

$$\frac{dV_s}{dt} = -\frac{V_s-(V-V_{bi})}{\tau_r} \quad (5)$$

Here V_{bi} is the built-in potential across the initial barrier, V_s is a surface voltage related to the internal surface charge (ions and holes), and τ_r is the relaxation time associated to the equilibration of the interface to external voltage, which is mainly regulated by ions kinetics as already described in relation to open circuit voltage decay above. A similar approach has been used to account for the observation of impedance loops in the IS spectra, and it is shown in Fig. 3d.[64] The simulations with this circuit generate impedance spectra typical from the PSC, two arcs and accumulation capacitance C_s, and new exotic features: inductive loops and negative capacitances which are related to the sluggish ion movement that retards surface polarization response. This is due to autonomous relaxation of the internal voltage, Eq. (5), that generates the inductive dynamics. The results of both surface polarization model fitting of *j-V* curves and equivalent circuit analysis by model in Fig. 3d show a very good agreement that establishes τ_r in the order of 20 s for measurements of different types of PSC at room temperature.

It was previously reported that negative capacitance effects are rather sensitive to the surface conditions,[65] and very large inductive effect was obtained in composite interfaces.[66] Recently other works have also stressed the connection of ionic-electronic accumulation at the surface, and its possible influence on electron transfer and

recombination rates, in order to explain large capacitance and inductive behaviour.[67-69] In the same spirit it was previously suggested that recombination is affected by ions.[70] Concerning the complexity of impedance spectroscopy response of perovskite solar cells, these approaches are focused in the right direction in providing explanations combining ionic and electronic features, however, the models remain at a fuzzy stage, so that important physical details cannot yet be verified. One study has provided a confirmation of negative capacitance[68] using older arguments for inductive response in the time domain.[71] It is worthwhile to mention that earlier approaches based on charge collection and modification of built-in electrical field in the bulk appeared to be abandoned in favor of the predominance of charging and reaction effects at the interface. Nevertheless, it must be remarked that capacitive features have to be explained in the frequency domain, as we need models that fit the IS data and produce quantitative conclusions. Indeed the recognized power of IS consists in the ability to use the spectra to separate features that cannot be well distinguished in the time domain. Therefore we need more spectral analysis, rather than less.

The topic of negative capacitance is an important part of the behaviour of many solar cell devices analyzed in the frequency domain.[72] “Negative capacitance” and “inductive behaviour” are widely accepted synonyms of a type of spectral behaviour, but the main effect associated to it, not so frequently noted, is that the resistance becomes smaller as the frequency decreases, causing the famous loops in the impedance spectra. This effect most often goes in the direction of decreasing the solar cell performance, particularly in perovskite solar cells,[73] and needs to be explained even on practical grounds.

However, this research topic is plagued by a basic problem. It is relatively easy to make some models that produce negative capacitance. There are some basic resources, that basically consist to introduce a cross-dependence in any regular electrochemical or semiconductor device model.[74, 75] To implement the method you make a rate constant depend on voltage, or you make one element in a circuit depend on the current elsewhere (there are endless possible variations), and in the small perturbation model you obtain a dephasing of ac current and voltage in which the model cannot be described by regular capacitors and resistors. In fact in such a model “capacitance” (as defined from the imaginary part of impedance Z) can become very large, or negative, resistance decreases at low frequency, and several things can happen, while causality holds. The reason is that such tricks, that represent very real phenomena in far from equilibrium situations, abandon the central diktat of detailed balance: the rule that the transition rates in nonequilibrium should be the same as those of equilibrium.[76] The cross-correlations introduced in the physical model violate this rule, thus thermodynamic quantities as the capacitance lose their ordinary meaning in the out-of – equilibrium situation. This is one reason why it is so easy to find “explanations” of the negative capacitance, and at the same time it is rather demanding to demonstrate experimentally a given coupling mechanism in such complex systems.

One promising approach is to combine different frequency modulated methods as IS

and IMPS, as these should give complementary spectral information that may reveal specific mechanisms.[77] For normal models obeying detailed balance, it was shown by Bertoluzzi and Bisquert that all these methods reduce to a common model that describes the different spectral responses.[78] In principle it appears that one method only should confirm the result of the other. However, a recent study by Ravishankar et al.[79] reveals an interesting outcome of this approach, see Fig. 3e. It was shown that the spectral coupling of resistances and capacitances is rather different in the separate IS and IMPS spectra. Therefore, IMPS can reveal three physical processes in cases where IS only shows two, due to the overlap of the effects of the separate contacts. This route will enable to obtain further information about the meaning of the low frequency resistances, in combination with complementary techniques.[35]

Nevertheless, the previous characterization methods suffer from the limitation that all the information is obtained from the physical measurement at the external contacts, without real internal spatial resolution. Thus it is important to adopt complementary methods. One important study by Weber and coworkers[80] of the distribution of charge carriers by Kelvin Probe Force Microscopy (KPFM) provided a direct demonstration of the strong ionic-electronic accumulation at the perovskite/TiO_2 contact, so that this is a fact that cannot be denied anymore. This was followed by detailed time transient study indicated in Figure 13.[24] They measured the time scale that is needed for charge redistribution of PSCs under operational condition and have found that the formation of localized interfacial charge occurred in a short time of 10 ms under illumination. However, after the light is switched off, the interfacial charge can stay over 500 ms which creates a slow response of photocurrent transient. A further detailed analysis of the contribution of ions and electronic charge shows that the weight of slow mobile ions on *j-V* hysteresis is quite small. Instead, the hysteresis is mainly caused by formation and desorption of interfacial charges.[24] Another important result of this paper is the explanation of a potential gradient related to electrical field as shown in Fig. 13b. Weber *et al.* showed that such potential distribution corresponds quantitatively to the tail of the double layer, as commented in Eq. (3), extended into the bulk due to a Debye length in the order of 200 nm, corresponding to background charge density of 10^{15} cm^{-3}, in excellent agreement with previous results of transient charging current.[29] The potential distribution along the bulk is an equilibrium feature, and the dominant kinetics is that of charging the interface.

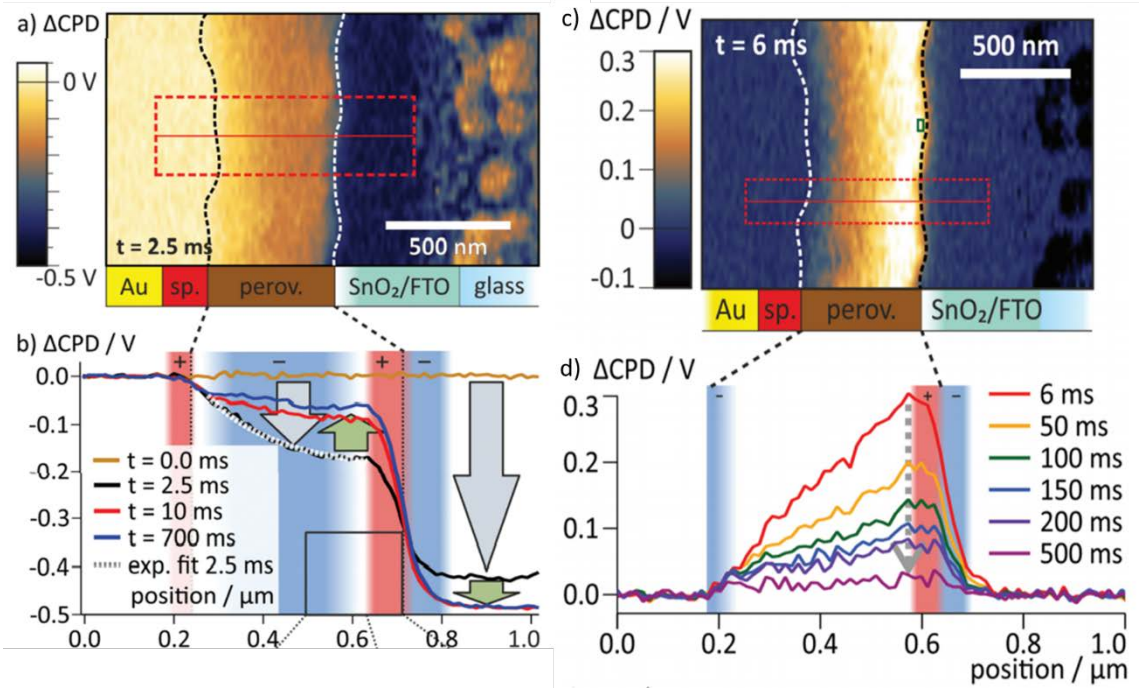

Figure 13. Time resolved KPFM results with pulsed illumination. (a) ΔCPD map 2.5 ms after the switching, where a strong potential gradient is present inside the perovskite. (b) Averaged ΔCPD sections from the rectangular area marked in a. (c) Map of ΔCPD measured 6 ms after switching off the voltage. The interfaces of the perovskite layer are marked with dotted lines. (d) Averaged section graphs obtained from the region indicated by the red box in (c) at different times after the switching. Adapted with permission from [24].

It should be mentioned that the very strong, well-recognized transient current associated to surface charging can affect the interpretation of galvanostatic techniques to separate ionic and electronic current contributions in planar samples with lateral contacts. This is why it is recommended to check the size of capacitances and to measure resistance instead of current in order to avoid gross misinterpretation, as remarked by Zhao et al.[81, 82]

Abate and coworkers have analyzed the long time behavior of the PSC under cycles of dark and illuminated state (Figure 14). In consonance with the evidence discussed above there is a transient behaviour that occurs between 10^{-1} and 10^{2} s that is associated to halide migration and accumulation at the electrode surface. In addition a much longer timescale phenomenon in the magnitude of 10^{3} s is attributed to cation migration that eventually leads to contact degradation. This result shows an extreme case in which slow migration does become important to control the kinetics of the PSC, in the case of the MA^{+} cation redistribution,[83] as indicated in Table 2.

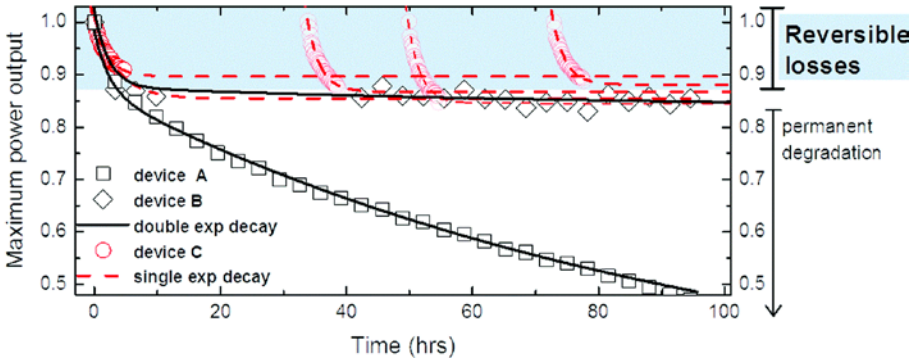

Figure 14. Maximum power output tracking for 3 identically prepared perovskite solar cells (device A, B and C) measured under UV-filtered 1 Sun equivalent light. Devices were continuously kept at the maximum power point using the standard "perturb and observe" method. Devices A and B were continuously tracked for over 100 hours. Device C was cyclically tracked 4 times for 5 hours and it was left in the dark at open circuit in between the consecutive measurements. Experimental data were fitted to an exponential decay (single or double). Reproduced with permission from [83].

In summary, there is a large component of capacitive current often observed but additional kinetic phenomena actuate at the same time and they need to be characterized. These additional phenomena have been described in the very low frequency domain (<1 Hz). We believe it is mandatory to obtain a full understanding of these effects even for technological reason. In fact, many claims of "suppressed hysteresis" may denote a successful slowing down of these effects to long times that are imperceptible in the typical range of laboratory measurement, but will nevertheless occur at real operation and practical times as in the example of Fig. 14.

Here we suggest that frequent observation of slow phenomena (<1 Hz) may be interpreted in many cases, beyond the charging-capacitive contribution, as the chemical interactions of ions in the perovskite that introduces a weak bond with the material at the contact, as suggested by Raman analysis in $MAPbI_3$-TiO_2 samples.[84] These detailed chemical interactions at interfaces are shown later in Section 9 on the perovskite/contact interface. Generally speaking the chemical interactions are material dependent and they lead to an additional delay on the time to release the ions being more costly than the surface polarization to build-up. In consequence, the surface polarization process introduces not just capacitive element but also a resistance, and both may be directly related not just by the charging of the double layer but also by surface absorption/reaction process. In this regard, it has been shown the remarkable result that the time constant in the range of 1 s is independent of illumination intensity and slightly dependent on cell thickness as shown in Fig. 15, and hence it is barely affected by the bulk electron concentrations. In order to explain these results, we need to adopt a more general point on view that embraces the dynamic phenomena observed both, in solar cells ca. 100 nm thick, and in much larger samples over 100 μm as described in the pioneering study by Almora, Guerrero and Garcia-Belmonte.[29]

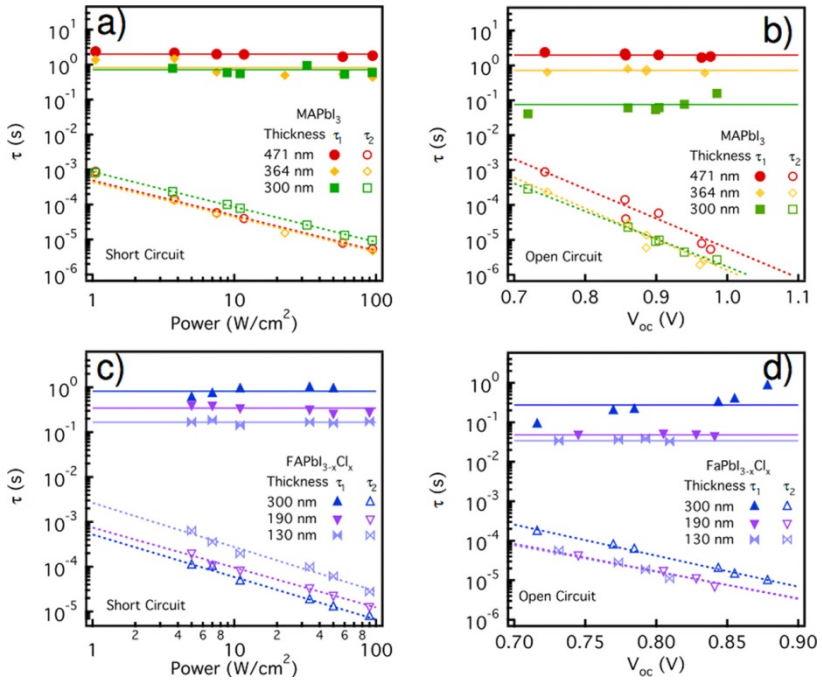

Figure 15. Response time calculated from the RC product for the low-frequency arc (solid line) and high-frequency arc (dashed line), respectively. (a) Short-circuit and (b) open-circuit conditions for $MAPbI_3$-based planar solar cells and (c) short-circuit and (d) open-circuit conditions for $FAPbI_{3-x}$ Cl_x-based planar solar cells. Reproduced with permission from [28].

The kinetic process that is characterized in the results of Fig. 15, is clearly related to the slow time constant in the 1 s domain that has been associated to a predominantly surface process related to ionic interaction with the surface. Nevertheless, the process presents a mixture of interfacial and bulk characteristics. This indicates that charging the double layer involves a transport for ions. Therefore the framework of separate time constants for transport and surface complexation suggested in Table 2 needs to be extended. Garcia-Belmonte et al. suggested[29] that the ion charging dynamics is composed of an average time for bulk transport in the thickness *d* and double layer charging as follows

$$\tau_{char} = \frac{L_D d}{D} \tag{6}$$

This approach is well established for liquid electrolytes and colloids.[85] In the case that $L_D \approx 200$ nm, for a distance d ≈ 400 nm the τ_{char} in Eq. (6) does not differ significantly from bulk diffusion as calculated in Table 2. However, Eq. (6) introduces a thickness-dependence in the time constant, as indicated by the solid line in Fig. 16, in agreement with the variations of time constant noted in Fig. 15. When the layer becomes much larger in the range of tens of μm, the effective time constants take values that cannot be explained by bulk diffusion while the dependence in Eq. (6) is in accord with

transient current results. [29] When we include the experimental results of Fig. 15 in the graph of Fig. 16, it is obvious that the experimental time constants become much larger than expected by simple double layer charging by diffusion as Eq. (6). This leads us to the previous conclusion that τ_{char} time is not explained simply by electrostatics and diffusion. The slow time constant contains these features but in addition, a significant component of surface binding, related to ionic relaxation suggested in Eq. (5), slows down the system, sets the value in the 1 s and longer domain, and eventually produces out-of-phase components leading to inductive behaviour in the frequency domain and a resistance that decreases at low frequency.

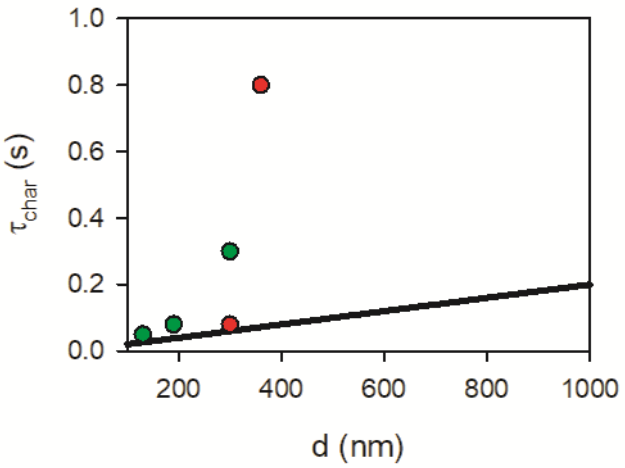

Figure 16. Representation of the ionic charging time for diffusion coefficient $D = 1 \times 10^{-8}$ cm^2 s^{-1} and Debye length $L_D = 200$ nm as a function of layer thickness. The points correspond to the data of Fig. 15 for $MAPbI_3$ (red) and $FAPbI_{3-x}Cl_x$ (blue).

Summarizing, we can provide a general perspective of kinetic studies discussed so far in PSCs, based on Fig. 3. Several general circuits have been provided, in most cases there are two basic processes, as in model b, at low and high frequency, which have been normally interpreted in terms of a bulk dielectric capacitance coupled with some resistance and a slow low frequency process fundamentally related to the interface. Nevertheless, some times by special experimental procedures three neat processes have been revealed, as in model c and e, which we believe correspond to a decoupling of the separate contacts. In addition it is often observed that the different resistances show correlated variations.

The low frequency process shows in many cases a constant kinetic time, as shown in Fig. 15, independent on current and voltage. Since the constant is a product RC, it occurs that the low frequency capacitance and resistance are correlated, which is very frequent in trapping models, and in silicon recombination, for example, in which the reciprocal dependence gives a fairly constant τ. However, the additional complexity in the PSC is that the low frequency features have combined properties of electronic and

ionic processes, then one can assume that capacitance is proportional to carrier densities $C_s \propto nc$ while for the resistance, which is inversely proportional to current, one has $R_1 \propto j^{-1} \propto (nc)^{-1}$. However, the specific coupling is rather uncertain, and complicates the understanding of the voltage distribution in PSC (from the separation of Fermi levels at the contacts). This is reflected by the uncertainty of models between series and parallel connection that becomes apparent when we combine the main models in Fig. 3. This limitation of the present understanding may be due to additional complexity that is starting to be revealed, as better and more robust samples become widely available, in comparison with early studies, were many random effects were introduced by the experimental itself. For example the hypothesis of a charging process along the bulk is well described in Eq. (6), but such process should correspond to a more complicated bulk diffusion with the kinetics indicated in model a of Fig. 3. Models for two or more carriers are not simply composed of series and parallel, so that circuits with two parallel lines, or with lumped elements are oversimplifications. Clearly there is a lot of room for careful experimental analysis and interpretation before a more complete picture can be established.

7. Mechanistic of Charging and Discharging of the Interfaces

There has been intensive efforts to use simulation techniques to predict the properties of the complete device stack as it is widely accepted that surface defects are a source of charge carrier trapping and will affect the extraction properties in photovoltaic devices.[86-88] Comprehensive reviews are available in the literature and detailed analysis is beyond the scope of this work.[89] From the atomistic point of view the different kinetics for charging and discharging are difficult to predict due to the large number of variables to take into account at the interface. Using the 3D periodic boundary condition, the surfaces can be modelled by a slab of a supercell, which consists of atomic layers and a vacuum layer. The interface of the perovskite with the contact is very rich as there can be different terminations; see for example three possible terminations in Figure 17a. To these terminations the twelve intrinsic point defects (vacancies, interstitials and the antisites) present in the bulk of the perovskite would also need to be taken into account at the interface.[90] For example, intrinsic point defect such as vacancies (V_I, V_{MA}, V_{Pb}), interstitials (I_i, Pb_i) and antisites (PbI, PbMA) were identified to be formed on each terminated surface, and their formation energies have been calculated for I-rich, moderate and Pb-rich conditions.[91] In addition, analysis of the different crystallization indices also leads to different results. Therefore, predicting the actual chemical reactions taking place at the interface is a very difficult task.

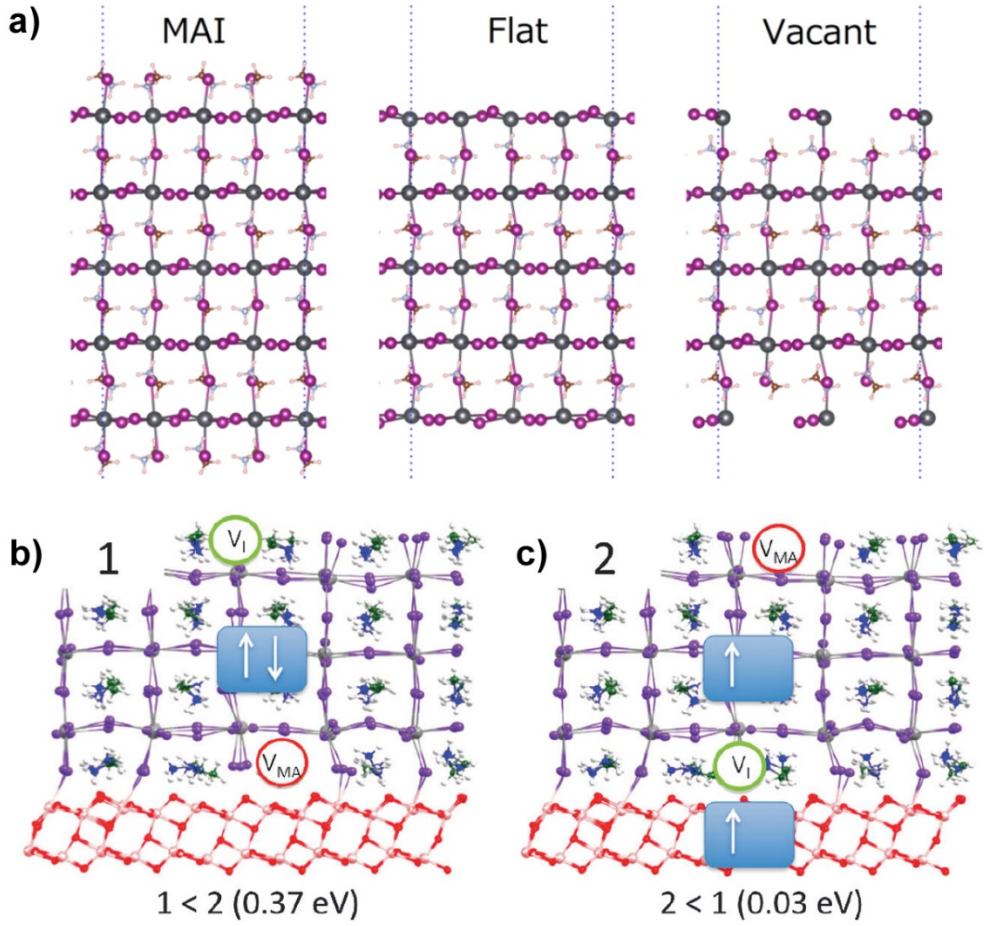

Figure 17. a) Examples of perovskite termination. Reproduced with permission from [91]. b) Location of V_I and V_{MA} in the ground state, VB edge localized on the perovskite and c) in the charge separated state in which one electron has been promoted from the perovskite to the TiO_2. Reproduced with permission from [92].

De Angelis *et al.* have intensively studied the TiO_2/$MAPbI_3$ interfaces using SOC-DFT calculations.[92, 93] It was revealed that by interactions of the perovskite with TiO_2 the interface adopts and electronic structure with strong coupling between the Ti 3d and Pb 6p conduction band states and upshifts the TiO_2 conduction band energy.[93] Defects at the interfaces (vacancies V_I and V_{MA}) were studied under working conditions and it was shown that vacancies V_I diffuse towards the HTL and V_{MA} towards the ETL side.[92] When compared with the non-defective interface, the outermost valence band states of the perovskite interfere with the band gap of the TiO_2, while the conduction band states are found inside the conduction states of the oxide. Overall, it was shown that defects at interfaces modify the band alignment, cause the bending of the perovskite bands close to the TiO_2 surface, and create the trap states.[92]

Due to the complexity of the system, the precise species formed at the interfaces during charging and discharging are difficult to predict. However, interfacial defects and migrating ions piling up at the contacts will lead to measurable double layer

capacitances, Helmholtz and diffuse layer. The sign and magnitude of the applied bias will modify the capacitance with time due to ion migration and to the chemical reactivity of migrating ions with the external contacts as it will be discussed below.[84] Figure 18 shows a simplistic view that highlights the direction of migration for only one ion as detected by capacitive current measurements in the dark. Due to the rich chemistry of iodine and to the presence of oxidative conditions once ions reach the external contacts these can react with the contact material, as described below, further modifying the capacitance. The kinetics of this type of reactions will be lower than that of ion migration since the availability of ions will be a requirement for the chemical reaction to take place. Therefore, chemical reactivity will be observed at long scale times (Figure 1) and low frequencies during impedance measurements.

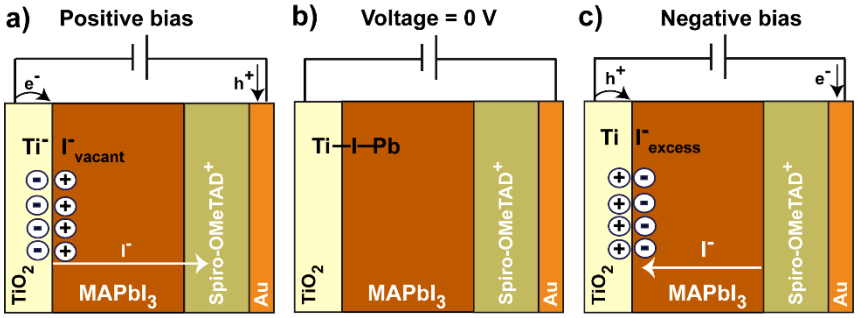

Figure 18. Diagrams representing iodide migration and chemical species present at the interfaces that lead to a modification in the capacitance. a) At positive bias iodine ions are forced to migrate towards the hole selective contact where the chemical reaction with *spiro*-OMeTAD$^+$ occurs. Iodine defective layer is formed at the TiO_2/$MAPbI_3$ interface. b) At zero bias neutral case appears. c) At negative bias *spiro*-OMeTAD only partially returns to its oxidized, conductive state. Iodine ions accumulate at the TiO_2. Reproduced with permission from [84].

8. Ferroelectric effects

There have been over the years different speculations on the influence of a ferroelectric property on PV behaviour of perovskite solar cells. Obtaining a permanent, switchable polarization in electrical insulators is relatively easy to determine by electrical methods. However, in the case of a metal halide perovskite semiconductor with contacts (necessary for PV application), there are intrinsic leakage currents and an ionic polarization component so that the true polar domain orientation is rather challenging to confirm.[94, 95] Recently the observation of ferroelectric polarization in the metal halide perovskites has been reported by different methods.[95-98] However, it is rather unclear that such property has any significance for PV properties. The use of ferroelectric materials in solar energy conversion has been reviewed elsewhere.[99] The application of an electrically polarized material as a solar cell aims to take benefit from charge separation by the electrical field. Most of the materials reported in the literature

are wide bandgap extreme insulators,[99] they provide tiny photocurrent, the polarization is always affected by a depolarising field, and the PV mechanism is rather uncertain in most cases: since electrical contacts normally shield the internal field, most observed characteristics are believed to be associated to contact properties. For example migration of defects can modify contact Schottky barriers by poling and produce a switchable characteristic of the photocurrent.[100, 101] In addition, charge separation is not a real issue in the metal halide perovskites that enjoy excellent semiconductor properties. Therefore the role of ferroelectric in PV behaviour should be rather minor.

Another potentially useful pathway to exploit the ferroelectric property is to build active thin switchable layers that improve the operation of contacts, or facilitates some type of memory device. In principle one can change the built-in voltage according to the state of the surface ferroelectric layer.[102] However, for low conductivity or depletion in the semiconductor the surface charge in the thin ferroelectric layer cannot be cancelled at the active material side. This situation leads to a large uncompensated field in the ferroelectric layer that will remove the polarization charge.[103] Recently this approach was realized for obtaining switchable response in perovskite solar cells,[104] but issues of charge compensation and ionic polarization make the interpretation of results rather difficult.

9. Perovskite/Contact interface: Chemical, structural and energetic properties

So far we have focused on the physical implications of ionic migration on material and device performance. In the following part, we consider the main types of chemical interactions at the perovskite/contact interface. Specifically we cover some morphological and chemical aspects that relate to kinetic charge distribution and thus require some attention to design a PSC stack with increased stability and without hysteresis.

It is well known that the property of interfaces is a dominant aspect of electronic devices such as solar cells. Therefore, lots of efforts have been devoted to develop the contacts in order to obtain high quality interfaces with desirable properties for high performance devices. The variety of contacts used as ETL and HTL in PSCs is almost endless and several recent reviews cover these aspects in detail.[3-5] In general, ETLs include metal oxides (i.e. TiO_2, SnO_2 or ZnO) or organic molecules (i.e. fullerenes). Similarly, materials used as HTLs also embrace metal oxides (i.e. NiO_x), CuSCN, CuI and organic compounds such as Spiro-OMeTAD, PEDOT:PSS or conductive carbon.[5, 105] We anticipate that chemically robust contacts are required to stand the highly reactive perovskite interface enabling efficient extraction of carriers. In general, electron/holes accumulation at the interface in the presence of migrating ions may lead to their degradation.

Morphology of contacts

Apart from all the chemical interactions the roughness of FTO substrate can also affect the hysteresis of PSCs as reported by Cojocaru *et al.*[106] Compared to the FTO with higher roughness, better device efficiency and relatively smaller hysteresis was obtained with the FTO with a flat surface. Because of the different roughness of FTO contact, the effect of surface treatment by $TiCl_4$ solution differs significantly, where $TiCl_4$ treatment showed effectiveness in a rough FTO surface compared to flat one. This is ascribed to the different surface contact degree with the perovskite as the flat FTO surface has better contact with the perovskite which ultimately leads to homogeneous accumulation of carriers at the interfaces.[106] Nanometer-scale in-situ current-voltage measurement used to detect the current flow at the interface of TiO_2/perovskite showed a tunneling current at TiO_2/perovskite interface when TiO_2 with rough surface was used, while such leak current was not observed with the TiO_2 with a smooth surface (Figure 19). The tunneling current was believed to be caused by the local-heavy doping due to electrostatic dipole at a rough TiO_2/perovskite interface, which triggers a chain reaction of charge accumulation and in turn causing a more severe hysteresis in the *j-V* plot.[107]

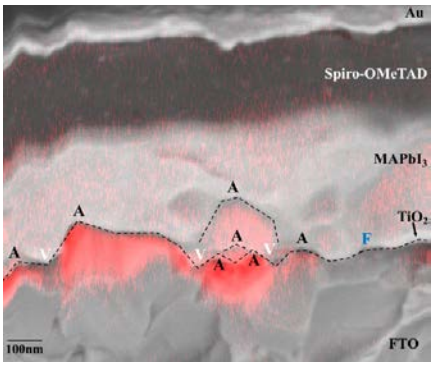

Figure 19. EBIC results showing the electron density map at apexes (black A), valleys (white V) and the flat interface (blue) F on a cross-sectional SEM image of a PSC. Reproduced with permission from [107].

Metal/perovskite contacts

There are several metals that have been used as the current collector layer in the device configuration such as Ca, Al, Ag, Au or Cr (Figure 20).[108] These contacts formed between metal and perovskite provide simple devices for mechanistic study. Perovskites have proved to oxidize the metals generating their corresponding halides (i.e. CaI_2, AlI_3 or AgI). For example, oxidation of Ag to form AgI has been widely studied by a range of techniques like XRD or XPS.[109]

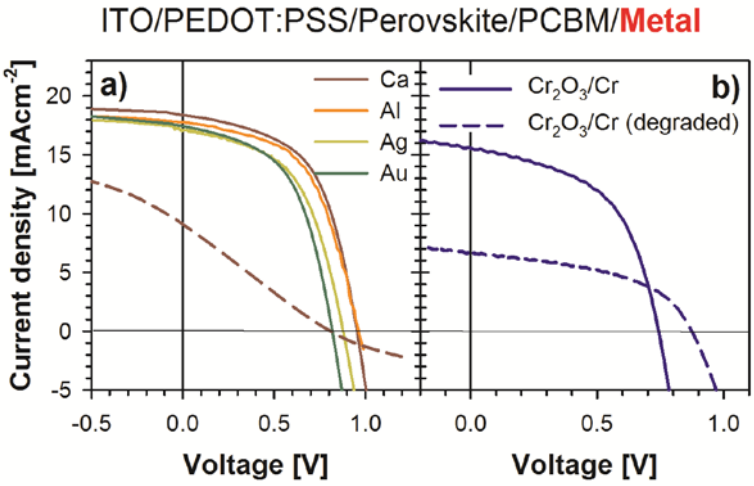

Figure 20. Current density-voltage curves of devices fabricated with different metal contacts measured at 1 sun light illumination. a) Metals providing S-shape curves after degradation b) Contact containing Cr_2O_2/Cr does not show S-shape after degradation. Degraded devices are shown as broken lines. Reproduced with permission from [108].

A mechanism as that shown in Figure 21 has been proposed in the presence of ambient water in which water reacts with the perovskite layer leading to formation of PbI_2 and subsequent iodine migration and surface diffusion form AgI. Even noble metals such as Au also lead to corrosion at the interface level under oxidative stress.[110] When used as a current collector with a buffer layer (i.e. Perovskite/ETL/Metal) a small area or pinhole not covered by the buffer layer is sufficient to lead to corrosion of the metal. In addition, due to the soft nature of the perovskite, metal diffusion through the perovskite has also been observed by analytical techniques like TOF-SIMMS.[111]

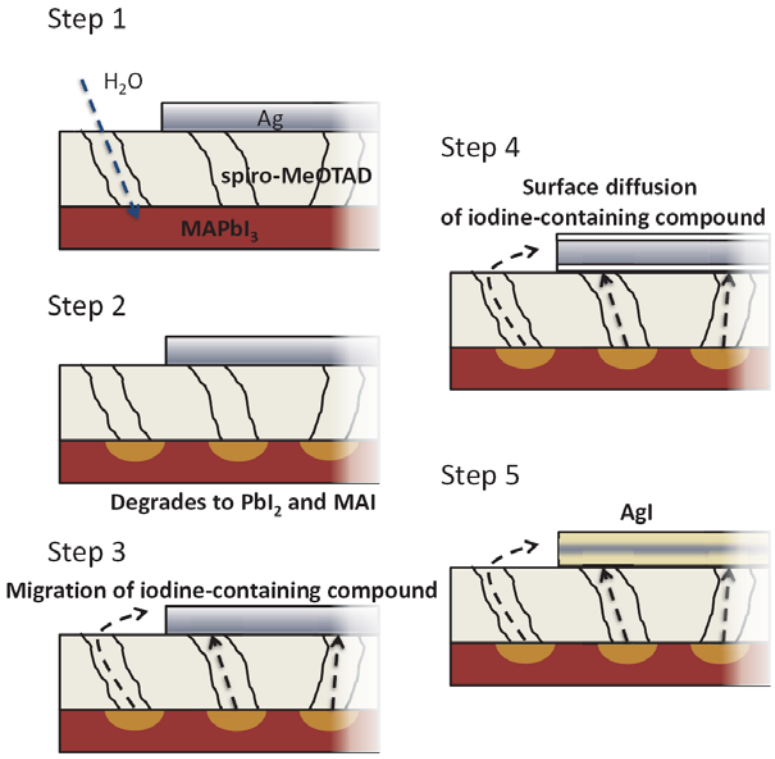

Figure 21. a) Proposed AgI formation mechanism in the presence of ambient water. Reproduced with permission from [109].

A thin buffer layer of chromium (Cr/Cr_2O_3) has proved to be very useful for stopping corrosion of the current collector.[112, 108] Tisdale *et al.* investigated the contact formed by $MAPbBr_3$ single crystals and metal Cr or Au. They have found that the contact between the perovskite/Cr is ohmic while when using Au to replace Cr, the contact property is switched to non-ohmic. Because of the different contact property, the perovskite/Cr showed a higher interfacial charge transfer resistance (R_{ct}) of 1.79×10^9 Ω compared to perovskite/Au ($R_{ct} = 1.32 \times 10^7$ Ω).[113] This is in contrast to the general understanding that the contact between the perovskite and Au is Ohmic.[114] Clearly more work is needed to understand the contact property of perovskite/contact for current collector materials such as metal, carbon etc, which is particularly important of HTL-free PSCs. Since Cr is very stable in the presence of iodine, it thus could be a promising electrical contact for PSCs to be considered in the future. The study on $MAPbBr_3$ single crystal in direct contact with ITO (or TiO_2) and Au based electrical contact (device structure: ITO/perovskite/Au or FTO/TiO_2/perovskite/Au) shows that, compared to TiO_2 based ETL, the ITO based PSC showed even higher J_{sc} (7.4 mA/cm^2 vs 7.0 mA/cm^2), but smaller V_{oc} (1.25 V vs 1.36 V) and FF (0.59 vs 0.69) in the reverse scan. In the forward scan, the ITO based device showed much poorer performance, leading to a very large hysteresis compared to the TiO_2 counterpart. The poor charge extraction at the interface of ITO/perovskite was blamed for this phenomenon.

ETL/perovskite interface and reactivity

TiO_2 is one of the most widely used electron transport material in PSCs, and some of its modification were already commented in section 5. Research has shown that TiO_2 is actually not an ideal ETL material in terms of energetic level matching the adjacent perovskite and stability under UV-light. Mesoporous TiO_2 was reported to have higher conduction band edge (E_{cb}) relative to that of perovskite $MAPbI_3$, causing inefficient interfacial charge injection. The periodic table has been scrutinized with several types of dopants for the TiO_2 layer. The general aim has been to improve the conductivity whilst not modifying greatly the band edges of TiO_2. The overall effect has been to improve the extraction properties of the contact and reduce recombination pathways. For example, TiO_2 has been doped with a wide variety of ions such as Li,[115] Ru,[116] Fe,[117] Co,[118] Y,[119] Cd,[120] La,[121] Sm, [122] Nb, [123] Er, [124] Ta,[125] Pt,[126] Zn,[127] Ga,[128], In,[129] or Sn[130]. Doping TiO_2 with alkaline cation such as lithium has been reported to improve its electronic properties such as reduced trap density, thus enhancing the dynamics of interfacial charge transfer.[131] Similarly, introduction of potassium cations (K^+) into the perovskite film has also demonstrated as an effective way to eliminate *j-V* hysteresis of PSCs. The location of K^+ in the perovskite crystal lattice is still under debate, but concrete experimental results show the conduction band edge of perovskite is shifted downward, leading to a more favourable energy alignment with SnO_2 for charge transfer.[132] Surface treatment of TiO_2 film with fluorine (CF_4)-based plasma was found to enhance the interface adhesion between the perovskite and the TiO_2.[133] The fluorine doped TiO_2 was also found to offer a more favourable energy alignment with adjacent perovskite material. Consequently, a dramatic improved device efficiency and reduced hysteresis in the *j-V* plot was achieved.

The metal oxide SnO_2 has lower conduction band and larger band gap (3.5-3.6 eV) than TiO_2, therefore it is normally considered that the charge transfer at SnO_2/perovskite is more efficient compared to TiO_2/perovskite. The pioneering work of Correa-Baena et al.[134] demonstrated the excellent properties of SnO_2 for planar contacts in PSC, in comparison to planar TiO_2, hence tin oxide has henceforth become a popular ETL in the planar cells. The subsequent study by impedance spectroscopy of the same cells[31] revealed enormous difference of dynamic properties and marked the standard models for IS in the literature, which is presented here in Fig. 3c. The material properties of the interface of SnO_x with halide perovskites, were characterized by Riedl, Olthof and coworkers,[135] who showed the spontaneous formation of a PbI_2 interfacial layer. An ETL based on a bilayer of compact crystalline-TiO_2/amorphous-SnO_2 was reported to enhance the charge extraction of PSCs and reducing hysteresis at the same time as a result of improved interface band alignment with triple cation $(Cs_{0.05}MA_{0.15}FA_{0.85}Pb(I_{0.85}Br_{0.15})_3$.[136]

The chemistry at the interfaces of PSC is responsible for many of the phenomena observed in the device. Limited research has indicated chemical reactions occurring at the interface of TiO_2/perovskite and perovskite/HTL. Raman spectrum of symmetrical

cell of FTO/TiO_2/perovskite/TiO_2/FTO has confirmed the formation of Ti-I-Pb bonds, which are able to accommodate accumulated charge, leading to capacitive current.[84] The highly reversible current-voltage plot indicate the process associated with charge storage of Ti-I-Pb is reversible. Generation of this type of chemical bonds is compatible with reactivity with Ti^{3+} defects present in the TiO_2 layer (Figure 22). Prevalent Ti^{3+} defects are present in TiO_2 in the tail of the conduction band and these defects are known to control the electronic response of some PV devices.[137] The dynamic response of the interface under light soaking experiments in organic PV clearly highlights that these defects are highly reactive and can interact with molecular oxygen. [138, 139]

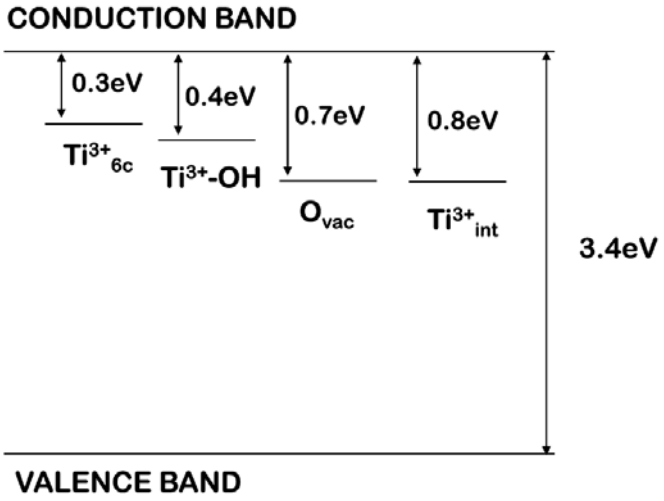

Figure 22. Schematic representation of the defect energy levels in the band gap of bulk anatase TiO_2 as derived from B3LYP calculations for the following Ti_{3+} species: (1) 6-fold-coordinated Ti_{6c3+}; (2) Ti_{6c3+}-OH species; (3) Ti_{5c3+} species associated with oxygen vacancies; and (4) interstitial $Ti_{5c\,3+}$ species. Reproduced with permission from [137].

The reversible chemical reactions at TiO_2/perovskite interfaces has also been proposed based on indirect evidence of reversible response showing chemical adsorption/desorption TiO_2/iodine gas and $MAPbI_3$/iodine gas which occurs in the time scale of seconds to minutes.[140] If the same reaction applies to the TiO_2/perovskite solid-solid interface, the proposed reversible reaction are:

$$e^-_{(TiO2)} + I^-_{ads\,(MAPbI3)} \Leftrightarrow I^-_{ads(TiO2)} + e^-_{(MAPbI3)} + trap^0_{(MAPbI3)}$$

These charge transfer reactions explain the large reversible capacitance observed with PSCs. Clearly the different surface defect property of TiO_2 can affect its reaction with I^- of $MAPbI_3$, thus the device performance and hysteresis. Therefore, apart from increasing the conductivity of the ETL other aspects like avoiding the reactivity of migrating ions with defects are required in order to control the *j-V* response and

stability.

Different methods have been reported to passivate the surface defects of TiO_2 by using small molecules such as PCBA, PCBM and C_{60}.[141] The surface modifier did not lead to change of morphology, crystallinity and bulk defect density of the perovskite layer that were deposited above the TiO_2 layer coated with the modifier. However, a more efficient charge extraction and recombination dynamics were observed at the interface of perovskite/ TiO_2-C_{60} compared to bare TiO_2, leading to much better performance and reduced hysteresis. An attempt to eliminate the current-voltage hysteresis of PSCs through tuning the interfacial chemical composition of perovskite/ETL by using a self-assembled monolayer (SAM) was also reported.[142] It was found that the PSCs had a thin layer of several-angstrom thick MAI-rich (Pb-poor) interface between the perovskite and the metal oxide, which caused formation of large capacitance and thus *j-V* hysteresis. By applying a self-assembled monolayer consisting of 6-octyl phosphonic acid (C6-PA)–C_{60}-C6-PA mixture above TiO_2 based ETL, the interfacial composition is switched from Pb-poor to Pb-rich while the property of the perovskite bulk was not affected. The chemical reactivity with TiO_2 is avoided in the SAM modified PSCs. This is explained by the capability of Pb-rich interface for compensating the ionic accumulated charge, therefore suppressing net charge at the interface and the capacitance, leading to elimination of the *j-V* hysteresis.

The important influence of interfacial chemical interaction on both performance and hysteresis of PSCs is also shown by Zou et al.[143] Using a series of SAM containing different functional group, they have found the chemical interaction between the SAM with perovskite dominates the device performance instead of energy position.[144] Polymer fullerene film (PMMA-PCBM) was found to effectively passivate defects at or near to the perovskite/TiO_2 interface, thus dramatically suppressing interfacial recombination. The interfacial passivation layer not only enhanced the V_{oc} of the cell up to 80 mV, but also removed the *j-V* hysteresis.[145] Patel *et al.* have found that the different interface contacts can affect the morphology of perovskite layers, which in turn affected the device performance and hysteresis. The study of vapor-deposited $MAPbI_3$ on four different ETL contact layers including compact TiO_2, C_{60}, compact TiO_2/PCBM and poly-TPD showed regions of amorphous $MAPbI_3$ close to the TiO_2 layer, which was attributed to the lattice mismatch between them. The amorphous $MAPbI_3$ at the interface led to poor charge collection and severe charge recombination, thus device hysteresis occurs via electrical capacitive effect.[146] This finding tells us the morphology change of perovskite in the presence of different contact should not be ignored when studying the hysteresis of PSCs.

Besides surface passivation, the interface property of ETL/perovskite can also be modified by tailoring the composition of the ETL. A recent work has shown that the *j-V* hysteresis of PSCs using SnO_2 as ETL could be related with density of oxygen vacancies in SnO_x film. By increasing the density of oxygen vacancy of SnO_2 thin film made by sputtering deposition through increasing annealing temperature, the efficiency

of PSCs was improved owing to significant enhanced V_{oc}. At the same time, the *j-V* hysteresis was substantially reduced.[147] Inorganic salt such as KCl was used to passivate the interface defects of SnO_2, which leads to a fast photocurrent response and an elongated lifetime. As a result, the efficiency of the device was enhanced while the hysteresis was suppressed.[143]

HTL/perovskite interface and reactivity

Similar to the ETL, the kinetics in the reactivity at the HTL/perovskite interface can determine the electrical response and stability of the device.[105] Nanoporous carbon electrodes developed by Han and coworkers is one of the most successful HTLs with the first report to show promising device stability exceeding 1000 h under full sun illumination.[148] The results indicated that the HTL material was compatible with the oxidative conditions generated in the perovskite layer and interface. In this process a stack containing mesoporous layers of different materials is filled with the perovskite precursor solution. Once the solvent is evaporated the perovskite forms inside the pores, whilst the interfacial chemistry will depend very much on the preparation method of the carbon ink. Hysteresis has been suppressed by controlling the thickness of the TiO_2 underlayer. It indicates that the carbon must have a small concentration of functional groups which can chemically interact with the migrating ions.[37]

Alternatively, if an organic HTL is deposited by solution processes on the top of the perovskite a thick layer of hundreds of nanometers will be required to avoid the exposure of the perovskite to the metal based current collector electrode. Due to the relatively low conductivity of the organic HTLs the use of additives is usually needed, which, however, give rise to some issues. On the one hand, lithium derivatives are used to stabilize oxidized species generated during light soaking of the Spiro-OMeTAD which increases the conductivity.[149, 150] On the other hand, bases like *tert*-butyl pyridine (tBP) an additive is usually used in Spiro-OMeTAD to tune the electronic properties of the layer. Unfortunately, both type of additives will interact with perovskite with Li^+ being able to migrate through the perovskite and the basic pyridine will coordinate to the lead atom of the perovskite.[23,151] For example, using time of flight secondary-ion mass spectroscopy (TOF-SIMS), a technique able to probe the chemical reactions at interfaces of PSCs, phase segregation and migration of extrinsic small cations like Li^+ was confirmed.[152] A gradient of A-site inorganic cations is observed in the perovskite film where it is rich at the back contact.[153] Meanwhile, degradation of perovskite due to the impact of tBP have been reported in literature.[154] It is believed the perovskite can react with tBP, resulting in formation of PbI_2-tBP intermediate and MAI product.

Very importantly, migrating ions in the perovskite layer will be able to react or diffuse into the HTL, leading to different responses. For example, the oxidized form of the widely used organic hole transport molecule Spiro-OMeTAD will lead to formation of the neutral iodine derivative Spiro-OMeTAD-I.[84] Of course, other side products will be generated which could in turn have their own impact. The reaction would be

irreversible, therefore causing permanent change/damage to the device performance including efficiency and stability.

$$\text{Spiro-OMeTAD}^{+} + I^{-} \rightarrow \text{Spiro-OMeTAD-I}$$

Stabilization of the cation leads to devices with increased stability in comparison with Spiro-OMeTAD as shown by Schloemer *et al.*[155] However, degradation is still severe under operation conditions. To avoid this type of reactivity, dopant-free HTLs have been designed by different groups. Brabec *et al.* have designed some conjugated polymers and have shown that the PDCBT derivative is a successful candidate able to stand oxidative conditions generated by I^{-}/I_3^{-} (Figure 25).[62, 156]

In addition, the use of metal oxides between the organic HTL and the current collector have been adopted with the aim to act as a physical barrier to stop ambient water diffusing into the device and the migration of iodine to the current collector.[156, 157] With this purpose MoOx and Ta-WOx have been used successfully. Reactivity of iodine with the current collector is reduced by having this additional layer as can be observed in Figure 23 and the stability in ambient conditions is enhanced.[157] However, an organic layer is needed at the interface between the perovskite and the metal oxide as otherwise there is a chemical reaction that form MoO_2 that reduces the ability of the system to extract charge.[158]

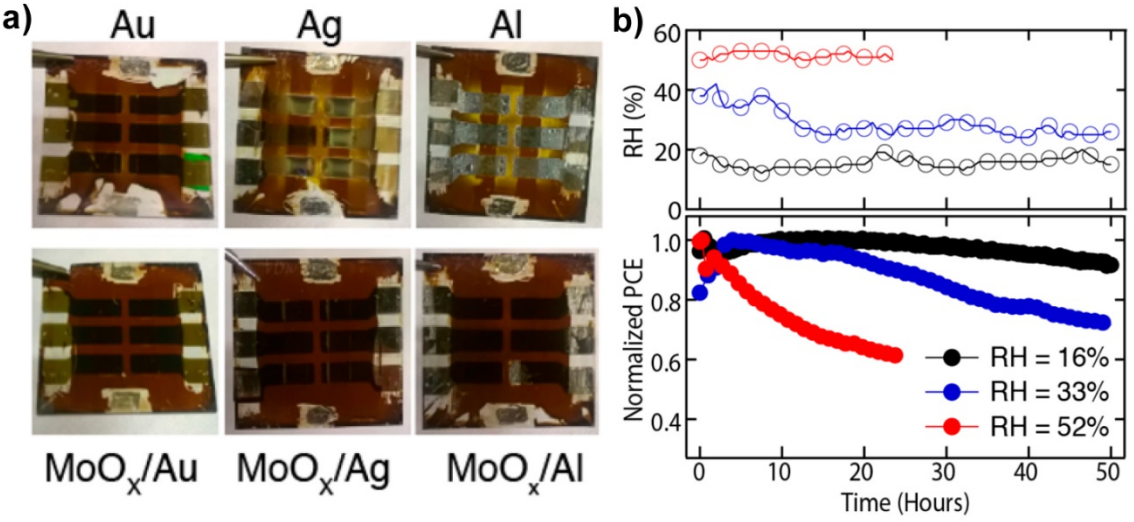

Figure 23. a) Optical images of devices containing different current collectors after 24 h of constant operation in ambient. b) Normalized PCE of similarly fabricated cells measured in three different RH conditions. All of the devices had the same electrode configuration of 15 nm of MoOx/200 nm of Al. Reproduced with permission from [157].

By careful alignment of conduction band of the perovskite and the HOMO level of the hole extraction layer, charge accumulation at the interfaces is avoided, thus reducing hysteresis and increasing the stability of the whole stack dramatically.[35] In the design of

the HTL it is important to tune the energy levels to stand towards oxidizing agents like I_2 that can be generated *in situ* by the migrating iodide ions and a high presence of holes.

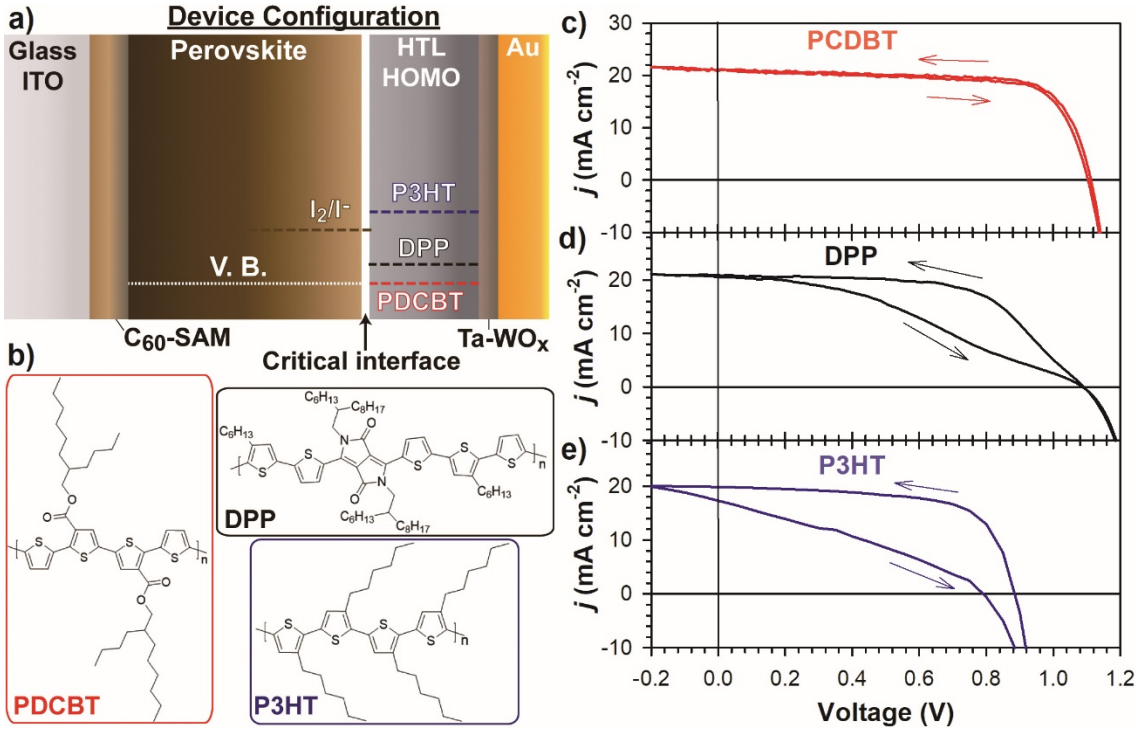

Figure 24. a) Device configuration where the HTL is the only parameter that has been modified. b) Chemical structure of different HTLs. c-e) *j-V* curves of PSCs with different HTLs. Reproduced with permission from [35].

Identification of chemical reactions in complete PSCs during lifetime

Perovskite solar cells are notorious for their unsatisfactory stability due to ease of degradation in the presence of water, oxygen, UV-light, external electrical bias, high temperature etc.[159] In this final section, we would like to highlight that during the lifetime of the PSCs several physical process and chemical reactions will be occurring simultaneously, each at their own timescale. Therefore, direct detection of the reaction product is a big challenge in practice and advanced analytical techniques are required to envisage the whole picture of the degradation processes. One representative example is provided by Sultana *et al.* who investigated degradation at the interface level in ambient with the design configuration ITO/ZnO/$MAPbI_3$/Spiro-OMeTAD/Ag.[160] Identification of degradation products from reaction at the interfaces of PSCs has been achieved using laser desorption/ionization mass spectroscopy (LDI-MS). These authors found that after two weeks, the perovskite decomposed to PbI_2. Meanwhile other products such as ZnI_2, PbO and AgI were also detected in the stability testing process. It is believed that the formation of PbO is caused by oxygen –mediated photo-reduction (Eq. 7a-7c). Besides PbO, another product in the degradation reaction is iodine (I_2). The formation of MA, HI and PbI_2 is a consequence of degradation of $MAPbI_3$ caused by water and oxygen (Eq.

7e-f).[87, 160]

$$PbI_2 + h\nu \rightarrow e^-_{cb}(PbI_2) + h^+_{vb}(PbI_2) \quad \textbf{(7a)}$$

$$e^-_{cb}(PbI_2) + O_2 \rightarrow O_2^{-\bullet} + PbI_2 \quad \textbf{(7b)}$$

$$(x+y)PbI_2 + y/2O_2^{-\bullet} \rightarrow (PbI_2)_x(PbO)_y + yI_2 \quad \textbf{(7c)}$$

$$2CH_3NH_3PbI_3 + 1/2O_2^{-\bullet} \rightarrow 2PbI_2 + 2CH_3NH_2 + H_2O + I_2 \quad \textbf{(7d)}$$

$$CH_3NH_3PbI_3 \xrightarrow{H_2O} CH_3NH_2 + PbI_2 + HI \quad \textbf{(7e)}$$

$$2CH_3NH_3I + 1/2O_2 \xrightarrow{h\nu} 2CH_3NH_2 + I_2 + H_2O \quad \textbf{(7f)}$$

Diffusion of HI to ZnO based ETL in the cell architecture leads to the formation of ZnI_2 (ZnO + HI $\rightarrow$$ZnI_2$ + H_2O). Meanwhile ZnI_2 can also be formed by reaction with MAI which is the product of the decomposition of $MAPbI_3$. Due to the presence of high concentration of electrons and holes and the reactivity of some of the reagent present in devices (i.e. oxygen, iodide), the redox chemistry also needs to be considered. Indeed, the oxidant iodine (I_2) has been reported to form in the device. They are responsible for formation of AgI (2Ag + I_2 = 2 AgI). The redox chemistry can be predicted by taking into account the position of the energy levels as shown Figure 25a. For example, Ag with a band full of electrons at -4.7 eV will favour the redox reaction with the oxidant system I^-/I_2 at ~5.0 eV. Similarly, reactivity with the oxidant iodine can also be a problem with the HTL. The reactivity of I^-/I_3^- with a series of three different HTL is monitored by color change of the HTL layers (Figure 25b-c).

Overall, understanding all the chemical processes occurring in a complete solar cells is a very challenging task. Not only acid-base chemistry needs to be considered in relation to the migrating ions but also redox and radical chemistry. Comprehensive analysis of the product as a result of interfacial reactions of complete PSC cell with different contacts can provide important information of the cause for device stability and *j-V* hysteresis. To date, such research is very limited. In the future, more work is clearly needed in this direction, in particular understanding the interface reactions of carbon based HTM-free perovskite may provide new insights into its working mechanism.

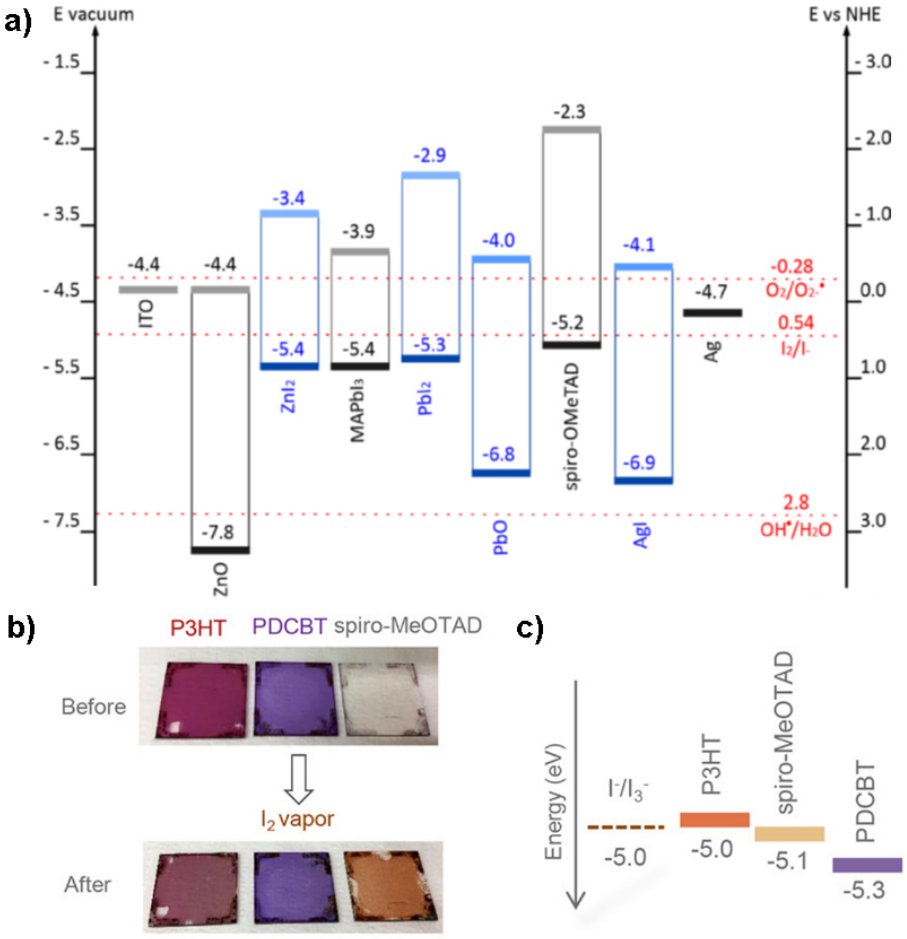

Figure 25. a) Energy level diagram of the material employed (black) and formed (blue) in the studied PSCs as well as potential of side redox reactions (red) occurring in the PSC. Reproduced with permission of [160]. b and c) Redox reactivity of different HTL with I^-/I3. Reproduced with permission of [156].

10. Conclusion and outlook

We have summarized evidence for surface charge and discharge phenomena at the contacts of the perovskite solar cell. Surface charge and discharge processes seem to follow markedly different kinetics, as in asymmetric trapping-detrapping associated with surface binding effects. On the one hand, supply of ions from the bulk of the perovskite material is fast under the effect of an electrical field or light. Ions will be transported to the contacts in the timescale of milliseconds for a typical semiconductor thickness of 100-200 nm. These ions will interact physically or chemically with the contacts generating an electrostatic potential. Depending on the nature of these interactions the release of the ions will be favoured (i.e. PCBM) or impeded (i.e. metal oxides). Ions present at the interface are detected by impedance spectroscopy as a very large surface capacitance that appears in the very low frequency domain. This capacitance clearly correlates with observed hysteresis during the *j-V* measurements. There are different

approaches to reduce this charge surface such as the use of interfacial layers at the perovskite/extraction layer or use of additives in the perovskite formulation. In general, the use of additives in the perovskite composition may show incorporation into the crystal lattice but the dynamic electrical properties seem to be related to the interfaces.

Acknowledgments

We thank financial support by Australian Research Council (ARC) through a discovery project (ARC DP 190102252) and Ministerio de Ciencia, Innovación y Universidades of Spain under project (MAT2016-76892-C3-1-R). A.G. would like to thank MICINN for a Ramón y Cajal Fellowship (RYC-201416809). Universitat Jaume I is also acknowledged for financial support (UJI-B2017-32).

1. D. Weber, *Z. Naturforsch. B*, 1978, **33**, 1443-1445.

2. A. Kojima, K. Teshima, Y. Shirai and T. Miyasaka, *J. Am. Chem. Soc.*, 2009, **131**, 6050-6051.

3. A. Fakharuddin, L. Schmidt-Mende, G. Garcia-Belmonte, R. Jose and I. Mora-Sero, *Adv. Energy Mater.*, 2017, **7**, 1700623.

4. B. Roose, Q. Wang and A. Abate, *Adv. Energy Mater.*, 2019, **9**, 1803140.

5. W. Zhou, Z. Wen and P. Gao, *Adv. Energy Mater.*, 2018, **8**, 1702512.

6. P. Schulz, *ACS Energy Lett.*, 2018, **3**, 1287-1293.

7. J. M. Azpiroz, E. Mosconi, J. Bisquert and F. De Angelis, *Energy Environ. Sci.*, 2015, **8**, 2118-2127.

8. T.-Y. Yang, G. Gregori, N. Pellet, M. Grätzel and J. Maier, *Angew. Chem. Int. Ed.*, 2015, **54**, 7905–7910.

9. I. Mora-Seró, G. Garcia-Belmonte, P. P. Boix, M. A. Vázquez and J. Bisquert, *Energy Environ. Sci.*, 2009, **2**, 678–686.

10. T. Kirchartz and U. Rau, in *Advanced Characterization Techniques for Thin Film Solar Cells*, eds. D. Abou-Ras, T. Kirchartz and U. Rau, Wiley, Berlin, 2011, p. 14.

11. Q. Wang, S. Ito, M. Grätzel, F. Fabregat-Santiago, I. Mora-Seró, J. Bisquert, T. Bessho and H. Imai, *J. Phys. Chem. B*, 2006, **110**, 19406-19411.

12. F. Fabregat-Santiago, J. Bisquert, E. Palomares, L. Otero, D. Kuang, S. M. Zakeeruddin and M. Grätzel, *J. Phys. Chem. C*, 2007, **111**, 6550-6560.

13. H. Wang and L. M. Peter, *J. Phys. Chem. C*, 2009, **113**, 18125-18133.

14. H. J. Snaith, A. Abate, J. M. Ball, G. E. Eperon, T. Leijtens, N. K. Noel, S. D. Stranks, J. T.-W. Wang, K. Wojciechowski and W. Zhang, *J. Phys. Chem. Lett.*, 2014, **5**, 1511-1515.

15. H.-S. Kim and N.-G. Park, *J. Phys. Chem. Lett.*, 2014, **5**, 2927-2934.

16. R. S. Sanchez, V. Gonzalez-Pedro, J.-W. Lee, N.-G. Park, Y. S. Kang, I. Mora-Sero and J. Bisquert, *J. Phys. Chem. Lett.*, 2014, **5**, 2357−2363.

17. V. T. Tiong, N. D. Pham, T. Wang, T. X. Zhu, X. L. Zhao, Y. H. Zhang, Q. Shen, J. Bell, L. H. Hu, S. Y. Dai and H. X. Wang, *Adv. Funct. Mater.*, 2018, **28**, 14.

18. C. Eames, J. M. Frost, P. R. F. Barnes, B. C. O'Regan, A. Walsh and M. S. Islam, *Nat. Commun.*, 2015, **6**, 7497

19. A. Senocrate, I. Moudrakovski, G. Y. Kim, T.-Y. Yang, G. Gregori, M. Grätzel and J. Maier, *Angew. Chem. Int. Ed.*, 2017, **56**, 7755-7759.

20. W. Peng, C. Aranda, O. M. Bakr, G. Garcia-Belmonte, J. Bisquert and A. Guerrero, *ACS Energy Lett.*, 2018, **3**, 1477-1481.

21. C. Li, A. Guerrero, S. Hüttner and J. Bisquert, *Nat. Commun.*, 2018, **9**, 5113.

22. L. M. Herz, *ACS Energy Lett.*, 2017, **2**, 1539-1548.

23. N. Vicente and G. Garcia-Belmonte, *Adv. Energy Mater.*, 2017, **7**, 1700710.

24. S. A. L. Weber, I. M. Hermes, S. H. Turren-Cruz, C. Gort, V. W. Bergmann, L. Gilson, A. Hagfeldt, M. Graetzel, W. Tress and R. Berger, *Energy Environ. Sci.*, 2018, **11**, 2404-2413.

25. F. Fu, T. Feurer, T. Jäger, E. Avancini, B. Bissig, S. Yoon, S. Buecheler and A. N. Tiwari, *Nat. Commun.*, 2015, **6**, 8932.

26. O. Almora, C. Aranda and G. Garcia-Belmonte, *J. Phys. Chem. C*, 2018, **122**, 13450-13454.

27. Z. Zolfaghari, E. Hassanabadi, D. Pitarch-Tena, S. J. Yoon, Z. Shariatinia, J. van de Lagemaat, J. M. Luther and I. Mora-Seró, *ACS Energy Lett.*, 2019, **4**, 251-258.

28. I. Zarazua, G. Han, P. P. Boix, S. Mhaisalkar, F. Fabregat-Santiago, I. Mora-Seró, J. Bisquert and G. Garcia-Belmonte, *J. Phys. Chem. Lett.*, 2016, **7**, 5105-5113.

29. O. Almora, A. Guerrero and G. Garcia-Belmonte, *Appl. Phys. Lett.*, 2016, **108**, 043903.

30. J. Bisquert, *Nanostructured Energy Devices: Equilibrium Concepts and Kinetics*, CRC Press, Boca Raton, 2014.

31. A. Guerrero, G. Garcia-Belmonte, I. Mora-Sero, J. Bisquert, Y. S. Kang, T. J. Jacobsson, J.-P. Correa-Baena and A. Hagfeldt, *J. Phys. Chem. C*, 2016, **120**, 8023-8032.

32. I. Zarazua, J. Bisquert and G. Garcia-Belmonte, *J. Phys. Chem. Lett.*, 2016, **7**, 525-528.

33. H.-S. Kim, I.-H. Jang, N. Ahn, M. Choi, A. Guerrero, J. Bisquert and N.-G. Park, *J. Phys. Chem. Lett.*, 2015, **6**, 4633–4639.

34. O. Almora, C. Aranda, I. Zarazua, A. Guerrero and G. Garcia-Belmonte, *ACS Energy Lett.*, 2016, **1**, 209-215.

35. V. K. Sangwan, M. Zhu, S. Clark, K. A. Luck, T. J. Marks, M. G. Kanatzidis and M. C. Hersam, *ACS Appl. Mater. Interfaces*, 2019, **11**, 14166–14174.

36. O. Almora, I. Zarazua, E. Mas-Marza, I. Mora-Sero, J. Bisquert and G. Garcia-Belmonte, *J. Phys. Chem. Lett.*, 2015, **6**, 1645-1652.

37. Y. G. Rong, Y. Hu, S. Ravishankar, H. W. Liu, X. M. Hou, Y. S. Sheng, A. Y. Mei, Q. F. Wang, D. Y. Li, M. Xu, J. Bisquert and H. W. Han, *Energy Environ. Sci.*, 2017, **10**, 2383-2391.

38. A. Guerrero, E. J. Juarez-Perez, J. Bisquert, I. Mora-Sero and G. Garcia-Belmonte, *Appl. Phys. Lett.*, 2014, **105**, 133902.

39. O. Almora, C. Aranda, E. Mas-Marzá and G. Garcia-Belmonte, *Appl. Phys. Lett.*, 2016, **109**, 173903.

40. D. Liu, Q. Wang, C. J. Traverse, C. Yang, M. Young, P. S. Kuttipillai, S. Y. Lunt, T. W. Hamann and R. R. Lunt, *ACS Nano*, 2018, **12**, 876-883.

41. C. Aranda, A. Guerrero and J. Bisquert, *ACS Energy Lett.*, 2019, **4**, 741-746.

42. C. S. Ponseca, T. J. Savenije, M. Abdellah, K. Zheng, A. Yartsev, T. Pascher, T. Harlang, P. Chabera, T. Pullerits, A. Stepanov, J.-P. Wolf and V. Sundström, *J. Am. Chem. Soc.*, 2014, **136**, 5189-5192.

43. S. van Reenen, M. Kemerink and H. J. Snaith, *J. Phys. Chem. Lett.*, 2015, **6**, 3808-3814.

44. P. Schulz, E. Edri, S. Kirmayer, G. Hodes, D. Cahen and A. Kahn, *Energy Environ. Sci.*, 2014, **7**, 1377-1381.

45. G. Yang, C. Wang, H. Lei, X. Zheng, P. Qin, L. Xiong, X. Zhao, Y. Yan and G. Fang, *J. Mat. Chem. A*, 2017, **5**, 1658-1666.

46. C. Quarti, F. De Angelis and D. Beljonne, *Chem. Mater.*, 2017, **29**, 958-968.

47. F. Zu, P. Amsalem, M. Ralaiarisoa, T. Schultz, R. Schlesinger and N. Koch, *ACS Appl. Mater. Interfaces*, 2017, **9**, 41546-41552.

48. S. Wang, T. Sakurai, W. Wen and Y. Qi, *Adv. Mater. Interfaces*, 2018, **5**, 1800260.

49. E. M. Miller, Y. Zhao, C. C. Mercado, S. K. Saha, J. M. Luther, K. Zhu, V. Stevanović, C. L. Perkins and J. van de Lagemaat, *Phys. Chem. Chem. Phys.*, 2014, **16**, 22122-22130.

50. D. Liu, S. Li, P. Zhang, Y. Wang, R. Zhang, H. Sarvari, F. Wang, J. Wu, Z. Wang and Z. D. Chen, *Nano Energy*, 2017, **31**, 462-468.

51. H. Tan, A. Jain, O. Voznyy, X. Lan, F. P. García de Arquer, J. Z. Fan, R. Quintero-Bermudez, M. Yuan, B. Zhang, Y. Zhao, F. Fan, P. Li, L. N. Quan, Y. Zhao, Z.-H. Lu, Z. Yang, S. Hoogland and E. H. Sargent, *Science*, 2017, **355**, 722.

52. F. Giordano, A. Abate, J. P. Correa Baena, M. Saliba, T. Matsui, S. H. Im, S. M. Zakeeruddin, M. K. Nazeeruddin, A. Hagfeldt and M. Graetzel, *Nat. Commun.*, 2016, **7**, 10379.

53. J. Wang, M. Qin, H. Tao, W. Ke, Z. Chen, J. Wan, P. Qin, L. Xiong, H. Lei, H. Yu and G. Fang, *Appl. Phys. Lett.*, 2015, **106**, 121104.

54. J.-Y. Seo, R. Uchida, H.-S. Kim, Y. Saygili, J. Luo, C. Moore, J. Kerrod, A. Wagstaff, M. Eklund, R. McIntyre, N. Pellet, S. M. Zakeeruddin, A. Hagfeldt and M. Grätzel, *Adv. Funct. Mater.*, 2018, **28**, 1705763.

55. N. D. Pham, C. Zhang, V. T. Tiong, S. Zhang, G. Will, A. Bou, J. Bisquert, P. E. Shaw, A. Du, G. J. Wilson and H. Wang, *Adv. Funct. Mater.*, 2019, **29**, 1806479.

56. C. H. Ng, T. S. Ripolles, K. Hamada, S. H. Teo, H. N. Lim, J. Bisquert and S. Hayase, *Sci. Rep.*, 2018, **8**, 2482.

57. S. Fantacci, F. De Angelis, M. K. Nazeeruddin and M. Grätzel, *J. Phys. Chem. C*, 2011, **115**, 23126-23133.

58. I. Gelmetti, N. F. Montcada, A. Pérez-Rodríguez, E. Barrena, C. Ocal, I. García-Benito, A. Molina-Ontoria, N. Martín, A. Vidal-Ferran and E. Palomares, *Energy Environ. Sci.*, 2019, **12**, 1309.

59. S. Ravishankar, S. Gharibzadeh, C. Roldán-Carmona, G. Grancini, Y. Lee, M. Ralaiarisoa, A. M. Asiri, N. Koch, J. Bisquert and M. K. Nazeeruddin, *Joule*, 2018, **2**, 788-798.

60. R. Gottesman, P. Lopez-Varo, L. Gouda, J. A. Jimenez-Tejada, J. Hu, S. Tirosh, A. Zaban and J. Bisquert, *Chem*, 2016, **1**, 776-789.

61. M. García-Rosell, A. Bou, J. A. Jiménez-Tejada, J. Bisquert and P. Lopez-Varo, *J. Phys. Chem. C*, 2018, **122**, 13920–13925.

62. A. Guerrero, A. Bou, G. Matt, O. Almora, T. Heumüller, G. Garcia-Belmonte, J. Bisquert, Y. Hou and C. Brabec, *Adv. Energy Mater.*, 2018, **8**, 1703376.

63. S. Ravishankar, O. Almora, C. Echeverría-Arrondo, E. Ghahremanirad, C. Aranda, A. Guerrero, F. Fabregat-Santiago, A. Zaban, G. Garcia-Belmonte and J. Bisquert, *J. Phys. Chem. Lett.*, 2017, **8**, 915-921.

64. E. Ghahremanirad, A. Bou, S. Olyaee and J. Bisquert, *J. Phys. Chem. Lett.*, 2017, **8**, 1402-1406.

65. A. Zohar, N. Kedem, I. Levine, D. Zohar, A. Vilan, D. Ehre, G. Hodes and D. Cahen, *J. Phys. Chem. Lett.*, 2016, **7**, 191-197.

66. M. Anaya, W. Zhang, B. C. Hames, Y. Li, F. Fabregat-Santiago, M. E. Calvo, H. J. Snaith, H. Miguez and I. Mora-Sero, *J. Mat. Chem. C*, 2017, **5**, 634-644.

67. D. Moia, I. Gelmetti, P. Calado, W. Fisher, M. Stringer, O. Game, Y. Hu, P. Docampo, D. Lidzey, E. Palomares, J. Nelson and P. R. F. Barnes, *Energy Environ. Sci.*, 2019, **12**, 1296.

68. F. Ebadi, N. Taghavinia, R. Mohammadpour, A. Hagfeldt and W. Tress, *Nat. Commun.*, 2019, **10**, 1574.

69. D. A. Jacobs, H. Shen, F. Pfeffer, J. Peng, T. P. White, F. J. Beck and K. R. Catchpole, *J. Appl. Phys.*, 2018, **124**, 225702.

70. A. Pockett and M. J. Carnie, *ACS Energy Lett.*, 2017, **2**, 1683-1689.

71. A. K. Jonscher, *J. Chem. Soc., Faraday Trans. 2*, 1986, **82**, 75-81.

72. I. Mora-Seró, J. Bisquert, F. Fabregat-Santiago, G. Garcia-Belmonte, G. Zoppi, K. Durose, Y. Y. Proskuryakov, I. Oja, A. Belaidi, T. Dittrich, R. Tena-Zaera, A. Katty, C. Lévy-Clement, V. Barrioz and S. J. C. Irvine, *Nano Lett.*, 2006, **6**, 640-650.

73. F. Fabregat-Santiago, M. Kulbak, A. Zohar, M. Vallés-Pelarda, G. Hodes, D. Cahen and I. Mora-Seró, *ACS Energy Lett.*, 2017, **2**, 2007-2013.

74. J. Bisquert, G. Garcia-Belmonte, A. Pitarch and H. Bolink, *Chem. Phys. Lett.*, 2006, **422**, 184-191.

75. J. Bisquert, *Phys. Chem. Chem. Phys.*, 2011, **13**, 4679-4685.

76. R. M. L. Evans, *Phys. Rev. Lett.*, 2004, **92**, 150601.

77. A. Pockett, G. E. Eperon, T. Peltola, H. J. Snaith, A. B. Walker, L. M. Peter and P. J. Cameron, *J. Phys. Chem. C*, 2015, **119**, 3456–3465.

78. L. Bertoluzzi and J. Bisquert, *J. Phys. Chem. Lett.*, 2017, **8**, 172-180.

79. S. Ravishankar, C. Aranda, S. Sanchez, J. Bisquert, M. Saliba and G. Garcia-Belmonte, *J. Phys. Chem. C*, 2019, **123**, 6444–6449.

80. V. W. Bergmann, Y. Guo, H. Tanaka, I. M. Hermes, D. Li, A. Klasen, S. A. Bretschneider, E. Nakamura, R. Berger and S. A. L. Weber, *ACS Appl. Mater. Interfaces*, 2016, **8**, 19402-19409.

81. W. Zhou, Y. Zhao, X. Zhou, R. Fu, Q. Li, Y. Zhao, K. Liu, D. Yu and Q. Zhao, *J. Phys. Chem. Lett.*, 2017, **8**, 4122-4128.

82. Y. Feng, Y. Zhao, W.-K. Zhou, Q. Li, W. A. Saidi, Q. Zhao and X.-Z. Li, *J. Phys. Chem. Lett.*, 2018, **9**, 6536-6543.

83. K. Domanski, B. Roose, T. Matsui, M. Saliba, S.-H. Turren-Cruz, J.-P. Correa-Baena, C. R. Carmona, G. Richardson, J. M. Foster, F. De Angelis, J. M. Ball, A. Petrozza, N. Mine, M. K. Nazeeruddin, W. Tress, M. Grätzel, U. Steiner, A. Hagfeldt and A. Abate, *Energy Environ. Sci.*, 2017, **10**, 604-613.

84. J. Carrillo, A. Guerrero, S. Rahimnejad, O. Almora, I. Zarazua, E. Mas-Marza, J. Bisquert and G. Garcia-Belmonte, *Adv. Energy Mater.*, 2016, **6**, 1502246.

85. M. Z. Bazant, K. Thornton and A. Ajdari, *Phys. Rev. E*, 2004, **70**, 021506.

86. W.-J. Yin, T. Shi and Y. Yan, *App. Phys. Lett.*, 2014, **104**, 063903.

87. J. M. Frost, K. T. Butler, F. Brivio, C. H. Hendon, M. van Schilfgaarde and A. Walsh, *Nano Lett.*, 2014, **14**, 2584-2590.

88. P. Umari, E. Mosconi and F. De Angelis, *Sci. Rep.*, 2014, **4**, 4467.

89. C.-J. Yu, *J. Phys. Energy*, 2019, **1**, 022001.

90. D. Meggiolaro, E. Mosconi and F. De Angelis, *ACS Energy Lett.*, 2018, **3**, 447-451.

91. H. Uratani and K. Yamashita, *J. Phys. Chem. Lett.*, 2017, **8**, 742-746.

92. J. M. Azpiroz, E. Mosconi, J. Bisquert and F. De Angelis, *Energy Environ. Sci.*, 2015, **8**, 2118-2127.

93. E. Mosconi, E. Ronca and F. De Angelis, *J. Phys. Chem. Lett.*, 2014, **5**, 2619-2625.

94. M. Coll, A. Gomez, E. Mas-Marza, O. Almora, G. Garcia-Belmonte, M. Campoy-Quiles and J. Bisquert, *J. Phys. Chem. Lett.*, 2015, **6**, 1408-1413.

95. Y. Rakita, O. Bar-Elli, E. Meirzadeh, H. Kaslasi, Y. Peleg, G. Hodes, I. Lubomirsky, D. Oron, D. Ehre and D. Cahen, *Proc. Natl. Acad. Sci. U. S. A.*, 2017, **114**, E5504-E5512.

96. L. M. Garten, D. T. Moore, S. U. Nanayakkara, S. Dwaraknath, P. Schulz, J. Wands, A. Rockett, B. Newell, K. A. Persson, S. Trolier-McKinstry and D. S. Ginley, *Sci. Adv.*, 2019, **5**, eaas9311.

97. H. Röhm, T. Leonhard, M. J. Hoffmann and A. Colsmann, *Energy Environ. Sci.*, 2017, **10**, 950-955.

98. Q. Zhang, A. Solanki, K. Parida, D. Giovanni, M. Li, T. L. C. Jansen, M. S. Pshenichnikov and T. C. Sum, *ACS Appl. Mater. Interfaces*, 2019, **11**, 13523–13532.

99. P. Lopez-Varo, L. Bertoluzzi, J. Bisquert, M. Alexe, M. Coll, J. Huang, J. A. Jimenez-Tejada, T. Kirchartz, R. Nechache, F. Rosei and Y. Yuan, *Phys. Rep.*, 2016, **653**, 1-40.

100. Y. S. Yang, S. J. Lee, S. Yi, B. G. Chae, S. H. Lee, H. J. Joo and M. S. Jang, *Appl. Phys. Lett.*, 2000, **76**, 774-776.

101. G.-L. Yuan and J. Wang, *Appl. Phys. Lett.*, 2009, **95**, 252904.

102. Y. Yuan, T. J. Reece, P. Sharma, S. Poddar, S. Ducharme, A. Gruverman, Y. Yang and J. Huang, *Nat. mater.*, 2011, **10**, 296-302.

103. K. Asadi, P. de Bruyn, P. W. M. Blom and D. M. de Leeuw, *Appl. Phys. Lett.*, 2011, **98**, 183301.

104. A. Pérez-Tomas, H. Xie, Z. Wang, H.-S. Kim, I. Shirley, S.-H. Turren-Cruz, A. Morales-Melgares, B. Saliba, D. Tanenbaum, M. Saliba, S. M. Zakeeruddin, M. Gratzel, A. Hagfeldt and M. Lira-Cantu, *Sustainable Energy Fuels*, 2019, **3**, 382-389.

105. Y. Yang, N. D. Pham, D. S. Yao, H. Y. Zhu, P. Yarlagadda and H. X. Wang, *Chin. Chem. Lett.*, 2018, **29**, 1242-1250.

106. L. Cojocaru, S. Uchida, P. V. V. Jayaweera, S. Kaneko, H. B. Wang, J. Nakazaki, T. Kubo and H. Segawa, *Energy Technol.*, 2017, **5**, 1762-1766.

107. T. W. Kim, M. Kim, L. Cojocaru, S. Uchida and H. Segawa, *ACS Energy Lett.*, 2018, **3**, 2743-2749.

108. A. Guerrero, J. You, C. Aranda, Y. S. Kang, G. Garcia-Belmonte, H. Zhou, J. Bisquert and Y. Yang, *ACS Nano*, 2016, **10**, 218–224.

109. Y. Kato, L. K. Ono, M. V. Lee, S. Wang, S. R. Raga and Y. Qi, *Adv. Mater. Interfaces*, 2015, **2**, 1500195.

110. V. Verdingovas, L. Müller, M. S. Jellesen, F. B. Grumsen and R. Ambat, *Corros. Sci.*, 2015, **97**, 161-171.

111. K. Domanski, J.-P. Correa-Baena, N. Mine, M. K. Nazeeruddin, A. Abate, M. Saliba, W. Tress, A. Hagfeldt and M. Grätzel, *ACS Nano*, 2016, **10**, 6306-6314.

112.M. Kaltenbrunner, G. Adam, E. D. Glowacki, M. Drack, R. Schwodiauer, L. Leonat, D. H. Apaydin, H. Groiss, M. C. Scharber, M. S. White, N. S. Sariciftci and S. Bauer, *Nat. Mater.*, 2015, **14**, 1032-1039.

113.J. T. Tisdale, E. Muckley, M. Ahmadi, T. Smith, C. Seal, E. Lukosi, I. N. Ivanov and B. Hu, *Adv. Mater. Interfaces*, 2018, **5**, 7.

114.W. Peng, L. F. Wang, B. Murali, K. T. Ho, A. Bera, N. Cho, C. F. Kang, V. M. Burlakov, J. Pan, L. Sinatra, C. Ma, W. Xu, D. Shi, E. Alarousu, A. Goriely, H. He, O. F. Mohammed, T. Wu and O. M. Bakr, *Adv. Mater.*, 2016, **28**, 3383-3390.

115.J. H. Heo, M. S. You, M. H. Chang, W. Yin, T. K. Ahn, S.-J. Lee, S.-J. Sung, D. H. Kim and S. H. Im, *Nano Energy*, 2015, **15**, 530-539.

116.S. Wang, B. Liu, Y. Zhu, Z. Ma, B. Liu, X. Miao, R. Ma and C. Wang, *Sol. Energy*, 2018, **169**, 335-342.

117.X. Gu, Y. Wang, T. Zhang, D. Liu, R. Zhang, P. Zhang, J. Wu, Z. D. Chen and S. Li, *J. Mater. Chem. C*, 2017, **5**, 10754-10760.

118.J. K. Kim, S. U. Chai, Y. Ji, B. Levy-Wendt, S. H. Kim, Y. Yi, T. F. Heinz, J. K. Nørskov, J. H. Park and X. Zheng, *Adv. Energy Mater.*, 2018, **8**, 1801717.

119.M. Li, Y. Huan, X. Yan, Z. Kang, Y. Guo, Y. Li, X. Liao, R. Zhang and Y. Zhang, *ChemSusChem*, 2018, **11**, 171-177.

120.Y. Li, Y. Guo, Y. Li and X. Zhou, *Electrochim. Acta*, 2016, **200**, 29-36.

121.X.-X. Gao, Q.-Q. Ge, D.-J. Xue, J. Ding, J.-Y. Ma, Y.-X. Chen, B. Zhang, Y. Feng, L.-J. Wan and J.-S. Hu, *Nanoscale*, 2016, **8**, 16881-16885.

122.Y. Xiang, Z. Ma, J. Zhuang, H. Lu, C. Jia, J. Luo, H. Li and X. Cheng, *J. Phys. Chem. C*, 2017, **121**, 20150-20157.

123.C. Liang, P. Li, Y. Zhang, H. Gu, Q. Cai, X. Liu, J. Wang, H. Wen and G. Shao, *J. Power Sources*, 2017, **372**, 235-244.

124.Z. Ren, J. Wu, N. Wang and X. Li, *J. Mater. Chem. A*, 2018, **6**, 15348-15358.

125.R. Ranjan, A. Prakash, A. Singh, A. Singh, A. Garg and R. K. Gupta, *J. Mater. Chem. A*, 2018, **6**, 1037-1047.

126.L.-L. Jiang, Z.-K. Wang, M. Li, C.-H. Li, P.-F. Fang and L.-S. Liao, *Sol. RRL*, **0**, 1800149.

127.H.-H. Wang, Q. Chen, H. Zhou, L. Song, Z. S. Louis, N. D. Marco, Y. Fang, P. Sun, T.-B. Song, H. Chen and Y. Yang, *J. Mater. Chem. A*, 2015, **3**, 9108-9115.

128.H. Liu, Z. Zhang, X. Zhang, Y. Cai, Y. Zhou, Q. Qin, X. Lu, X. Gao, L. Shui, S. Wu and J.-M. Liu, *Electrochim. Acta*, 2018, **272**, 68-76.

129.J. Peng, T. Duong, X. Zhou, H. Shen, Y. Wu, H. K. Mulmudi, Y. Wan, D. Zhong, J. Li, T. Tsuzuki, K. J. Weber, K. R. Catchpole and T. P. White, *Adv. Energy Mater.*, 2017, **7**, 1601768.

130.Q. Cai, Y. Zhang, C. Liang, P. Li, H. Gu, X. Liu, J. Wang, Z. Shentu, J. Fan and G. Shao, *Electrochim. Acta*, 2018, **261**, 227-235.

131.F. Giordano, A. Abate, J. P. C. Baena, M. Saliba, T. Matsui, S. H. Im, S. M. Zakeeruddin, M. K. Nazeeruddin, A. Hagfeldt and M. Graetzel, *Nat. Commun.*, 2016, **7**, 10379.

132.D. S. Yao, C. M. Zhang, N. D. Pham, Y. H. Zhang, V. T. Tiong, A. J. Du, Q. Shen, G. J. Wilson and H. X. Wang, *J. Phys. Chem. Lett.*, 2018, **9**, 2113-2120.

133.V. Zardetto, F. di Giacomo, H. Lifka, M. A. Verheijen, C. H. L. Weijtens, L. E. Black, S. Veenstra, W. M. M. Kessels, R. Andriessen and M. Creatore, *Adv. Mater. Interfaces*, 2018, **5**, 6.

134.J. P. Correa-Baena, L. Steier, W. Tress, M. Saliba, S. Neutzner, T. Matsui, F. Giordano, T. J. Jacobsson, A. R. Srimath Kandada, S. M. Zakeeruddin, A. Petrozza, A. Abate, M. K. Nazeeruddin, M. Gratzel and A. Hagfeldt, *Energy Environ. Sci.*, 2015, **8**, 2928-2934.

135.T. Hu, T. Becker, N. Pourdavoud, J. Zhao, K. O. Brinkmann, R. Heiderhoff, T. Gahlmann, Z. Huang, S. Olthof, K. Meerholz, D. Többens, B. Cheng, Y. Chen and T. Riedl, *Adv. Mater.*, 2017, **29**, 1606656.

136.M. M. Tavakoli, P. Yadav, R. Tavakoli and J. Kong, *Adv. Energy Mater.*, 2018, **8**, 9.

137.C. Di Valentin, G. Pacchioni and A. Selloni, *J. Phys. Chem. C*, 2009, **113**, 20543-20552.

138.H. Schmidt, K. Zilberberg, S. Schmale, H. Flügge, T. Riedl and W. Kowalsky, *Appl. Phys. Lett.*, 2010, **96**, 243305.

139.A. Guerrero, S. Chambon, L. Hirsch and G. Garcia-Belmonte, *Adv. Funct. Mater.*, 2014, **24**, 6234-6240.

140.R. A. Kerner and B. P. Rand, *J. Phys. Chem. Lett.*, 2017, **8**, 2298-2303.

141.K. K. Wong, A. Fakharuddin, P. Ehrenreich, T. Deckert, M. Abdi-Jalebi, R. H. Friend and L. Schmidt-Mende, *J. Phys. Chem. C*, 2018, **122**, 10691-10698.

142.J. Will, Y. Hou, S. Scheiner, U. Pinkert, I. M. Hermes, S. A. L. Weber, A. Hirsch, M. Halik, C. Brabec and T. Unruh, *ACS Appl. Mater. Interfaces*, 2018, **10**, 5511-5518.

143.X. Liu, Y. F. Zhang, L. Shi, Z. H. Liu, J. L. Huang, J. S. Yun, Y. Y. Zeng, A. B. Pu, K. W. Sun, Z. Hameiri, J. A. Stride, J. Seidel, M. A. Green and X. J. Hao, *Adv. Energy Mater.*, 2018, **8**.

144.L. J. Zuo, Q. Chen, N. De Marco, Y. T. Hsieh, H. J. Chen, P. Y. Sun, S. Y. Chang, H. X. Zhao, S. Q. Dong and Y. Yang, *Nano Lett.*, 2017, **17**, 269-275.

145.J. Peng, Y. Wu, W. Ye, D. A. Jacobs, H. Shen, X. Fu, Y. Wan, T. Duong, N.

Wu, C. Barugkin, H. T. Nguyen, D. Zhong, J. Li, T. Lu, Y. Liu, M. N. Lockrey, K. J. Weber, K. R. Catchpolea and T. P. White, *Energy Environ. Sci.*, 2017, **10**, 1792-1800.

146.J. B. Patel, J. Wong-Leung, S. Van Reenen, N. Sakai, J. T. W. Wang, E. S. Parrott, M. Z. Liu, H. J. Snaith, L. M. Herz and M. B. Johnston, *Adv. Electron. Mater.*, 2017, **3**, 6.

147.F. Ali, N. D. Pham, H. J. Bradford, N. Khoshsirat, K. Ostrikov, J. M. Bell, H. Wang and T. Tesfamichael, *ChemSusChem*, 2018, **11**, 3096-3103.

148.A. Mei, X. Li, L. Liu, Z. Ku, T. Liu, Y. Rong, M. Xu, M. Hu, J. Chen, Y. Yang, M. Grätzel and H. Han, *Science*, 2014, **345**, 295-298.

149.U. B. Cappel, T. Daeneke and U. Bach, *Nano Lett.*, 2012, **12**, 4925-4931.

150.R. S. Sanchez and E. Mas-Marza, *Sol. Energy Mater. Sol. Cells*, 2016, **158**, 189-194.

151.Z. Li, C. Xiao, Y. Yang, S. P. Harvey, D. H. Kim, J. A. Christians, M. Yang, P. Schulz, S. U. Nanayakkara, C.-S. Jiang, J. M. Luther, J. J. Berry, M. C. Beard, M. M. Al-Jassim and K. Zhu, *Energy Environ. Sci.*, 2017, **10**, 1234-1242.

152.Z. Li, C. X. Xiao, Y. Yang, S. P. Harvey, D. H. Kim, J. A. Christians, M. J. Yang, P. Schulz, S. U. Nanayakkara, C. S. Jiang, J. M. Luther, J. J. Berry, M. C. Beard, M. M. Al-Jassim and K. Zhu, *Energy Environ. Sci.*, 2017, **10**, 1234-1242.

153.S. P. Harvey, Z. Li, J. A. Christians, K. Zhu, J. M. Luther and J. J. Berry, *ACS Appl. Mater. Interfaces*, 2018, **10**, 28541-28552.

154.Y. F. Yue, N. Salim, Y. Z. Wu, X. D. Yang, A. Islam, W. Chen, J. Liu, E. B. Bi, F. X. Xie, M. L. Cai and L. Y. Han, *Adv. Mater.*, 2016, **28**, 10738.

155.T. H. Schloemer, T. S. Gehan, J. A. Christians, D. G. Mitchell, A. Dixon, Z. Li, K. Zhu, J. J. Berry, J. M. Luther and A. Sellinger, *ACS Energy Lett.*, 2019, **4**, 473-482.

156.Y. Hou, X. Du, S. Scheiner, D. P. McMeekin, Z. Wang, N. Li, M. S. Killian, H. Chen, M. Richter, I. Levchuk, N. Schrenker, E. Spiecker, T. Stubhan, N. A. Luechinger, A. Hirsch, P. Schmuki, H.-P. Steinrück, R. H. Fink, M. Halik, H. J. Snaith and C. J. Brabec, *Science*, 2017, **358**, 1192-1197.

157.E. M. Sanehira, B. J. Tremolet de Villers, P. Schulz, M. O. Reese, S. Ferrere, K. Zhu, L. Y. Lin, J. J. Berry and J. M. Luther, *ACS Energy Lett.*, 2016, **1**, 38-45.

158.P. Schulz, J. O. Tiepelt, J. A. Christians, I. Levine, E. Edri, E. M. Sanehira, G. Hodes, D. Cahen and A. Kahn, *ACS Appl. Mater. Interfaces*, 2016, **8**, 31491-31499.

159.M. Shahbazi and H. X. Wang, *Sol. Energy*, 2016, **123**, 74-87.

160.N. Sultana, N. J. Demarais, D. Shevchenko and P. J. Derrick, *Sol. RRL*, 2018, **2**, 9.